Siliciclastic prelude to Elatina–Nuccaleena deglaciation: lithostratigraphy and rock magnetism of the base of the Ediacaran system

T. D. RAUB, D. A. D. EVANS & A. V. SMIRNOV

Department of Geology and Geophysics, Yale University, New Haven, CT 06520-8109 USA (e-mail: timothy.raub@yale.edu)

Abstract: The basal Ediacaran global boundary stratotype section and point (GSSP) horizon beneath Nuccaleena Formation cap dolostone in South Australia's central Flinders Ranges South Australia coincides with an interpreted unconformity preceding deglacial transgression. Detailed lithostratigraphy of three sections across the base of the Ediacaran System at its type area reveals contrasting character of the Elatina Formation—Nuccaleena Formation transition across *c.* 9 km of exposure, changing the interpretive context of the GSSP.

We suggest that a locally pervasive, incisive flaser-bedded sandstone exposed between Elatina diamictites and Nuccaleena cap dolostone lies above an unconformity that correlates with the defined base of Wilpena Group, reflecting onset of terminal Elatina 'Snowball Earth' deglaciation and dynamic interplay between eustatic sea level change and isostatic rebound. Nuccaleena cap dolostone is sedimentologically mixed and conformable with underlying siliciclastics at Elatina Creek; hence the recently defined Ediacaran GSSP horizon, at the base of solid cap carbonate at Enorama Creek, lies in continuous section and not at an unconformity.

Nuccaleena Formation cap dolostone contains pervasive terrigenous debris, including apparently detrital hematite. While magnetite and/or maghemite is produced in abundance upon heating of the cap carbonate above *c.* 400°C, and we cannot exclude secondary origin of any Nuccaleena magnetite, Nuccaleena Formation cap dolostone should preserve primary magnetization.

Cap carbonates overlying late Neoproterozoic glacial rocks in Australia, and presumed correlative supraglacial carbonates around the world, are considered to record the aftermath of a glaciation of Marinoan age (widely termed 'Marinoan glaciation' e.g. Kennedy 1996; Kennedy *et al.* 1998; Evans 2000; Hoffman & Schrag 2002; here termed 'Elatina glaciation' to emphasize region-specific, and not necessarily globally-generalizable implications, for 'Snowball Earth' climate dynamics). In South Australia's Adelaide Rift Complex, the type-Marinoan Series (Preiss 1987, 1993, 2000) includes ferric siliciclastic units correlated to Elatina Formation, which variably exhibit undeniably glaciogenic facies (Lemon & Gostin 1990) deposited at low palaeolatitude (Embleton & Williams 1986; Sumner *et al.* 1987; Schmidt *et al.* 1991; Schmidt & Williams 1995; Sohl *et al.* 1999).

Although Lemon & Gostin (1990) considered all Elatina Formation in central Flinders Ranges as deposited following peak glaciation, subsequent development of 'hard' (e.g. Hoffman *et al.* 1998; Hoffman & Schrag 2002; Goodman & Pierrehumbert 2003; Halverson *et al.* 2004; Bodiselitch *et al.* 2005; Hoffman *et al.* 2005; Kasemann *et al.* 2005; Pollard & Kasting 2005; Pierrehumbert 2005) and 'soft' (e.g. Kirschvink 1992; Hyde *et al.* 2000; Kennedy *et al.* 2001) 'Snowball Earth' hypotheses offer considerable interpretive flexibility for assigning stratigraphic intervals of either monotonic or alternating waxing and waning to the Elatina ice age. Frequently, terminal Elatina deglaciation is hypothesized to begin during a depositional hiatus between the Elatina Formation and the overlying Nuccaleena Formation, at a level where siliciclastics traditionally assigned to Elatina Formation and equivalents in central Flinders Ranges contact 'cap' dolostone of Nuccaleena Formation (e.g. Christie-Blick *et al.* 1995; Kennedy 1996; implied as the base of the cap carbonate transgressive system tract by Knoll *et al.* 2004; Knoll *et al.* 2006; though Hoffman 2005 and Nogueira *et al.* 2003 interpret minimal hiatus beneath cap carbonates in Namibia and Brazil, respectively). For extended discussion of Elatina Formation, Nuccaleena Formation, and hypothesized correlative lithofacies outside central Flinders Ranges, see Preiss (1992), Preiss *et al.* (1998) and Preiss (2000).

The first part of this paper modifies this definition by placing the basal Nuccaleena Formation sequence boundary within siliciclastics that has been traditionally assigned to the Elatina Formation beneath Nuccaleena Formation cap dolostone, an interpretation permitted, though not explicated, by Lemon & Gostin (1990). The threefold division and basinal correlation of Elatina Formation by

From: VICKERS-RICH, P. & KOMAROWER, P. (eds). *The Rise and Fall of the Ediacaran Biota.* Geological Society, London, Special Publications, **286**, 53–76.
DOI: 10.1144/SP286.5 0305-8719/07/$15.00

those authors, modified and extended by Preiss (1992, 2000) and Preiss *et al.* (1998) may readily fit the observations described here if this basal Nuccaleena Formation siliciclastic facies is unique, or if it correlates with Seacliff sandstone. This siliciclastic unit may also correlate with uppermost Reynella siltstone or uppermost Ketchowla siltstone, if deposition persisted in the Oraparinna diapir salt-withdrawal syncline during erosion or non-deposition of coeval strata in the type-areas of those members. This condition is required in order to permit observed unconformity of Wilpena Group atop Elatina Formation equivalents in those locations. All three possibilities are discussed later; with the first two preferred over the third.

Nuccaleena Formation cap dolostone

Throughout Adelaide Rift Complex, Nuccaleena Formation is reported to show several contact relations with underlying siliciclastics. As summarized by Preiss (1987, 1992, 2000) and Preiss *et al.* (1998), the Umberatana Group—Wilpena Group boundary is a fundamental erosional surface, and the bedding of basal Wilpena Group Nuccaleena Formation or Brachina Formation equivalents is frequently low-angle discordant and only locally concordant with Elatina-correlative siliciclastics. Where concordant, the basal Nuccaleena contact is generally sharp, often recessive, and in places disconformable above an uppermost-Elatina pebble-bearing lag deposit. Lemon & Gostin (1990) interpret rare, calcareous-weathering Elatina horizons within centimetres of basal Nuccaleena Formation cap dolostone at the Enorama Creek GSSP as an exceptional 'gradational' (more accurately, mixed) formational transition. Subsequent workers tend to favour invoking Nuccaleena-age diagenetic carbonate fronts invading downward through pre-deposited siliciclastics to create layering at this particular outcrop (N. Christie-Blick and J. Gehling, pers. comm. 2004).

In light of the global expression of late Neoproterozoic 'Snowball Earth' cap carbonates, these collective indications of unconformity at the base of Nuccaleena Formation cap dolostone were used to construct a close approximation of a globally synchronous surface, thereby defining the Ediacaran Period GSSP at the base of solid cap carbonate in Enorama Creek, central Flinders Ranges, South Australia (Christie-Blick *et al.* 1995; Knoll *et al.* 2004; Knoll *et al.* 2006). Observations described in this paper demonstrate that, at least in the GSSP-hosting Oraparinna diapir salt-withdrawal syncline, the unconformity more accurately lies within defined Elatina Formation; and Nuccaleena Formation (basal Wilpena Group) must be redefined downward to contain initial siliciclastic lithofacies. The Enorama Creek GSSP horizon, consequently, need not be considered controversial for occupying an assumed unconformable surface.

Generally, Nuccaleena Formation cap dolostone varies in thickness and continuity of character. Where dominated by nearly continuous, low-angle to parallel-bedded peloidal dolomicrite in central Flinders Ranges, Nuccaleena Formation cap dolostone is everywhere at least 75 cm thick and ranges to approximately 10 metres, averaging about 3–4 m. Discontinuous expression of carbonate spans *c.* 50 m near Leigh Creek (Preiss 1987). The typical <10 m thick Nuccaleena Formation cap dolostone of central Flinders Ranges conveniently corresponds to the best-understood outcrop belt of demonstrably glaciogene, underlying Elatina facies, which has received focus in early studies, particularly that of Lemon & Gostin (1990). For that reason, although further complications of the Elatina–Nuccaleena transition interval across the basin may be anticipated or unresolved, this paper restricts focus to three sections in a continuous outcrop belt along the western homocline of the central Flinders zone in order to reassess the Elatina terminal-deglacial palaeoenvironment.

Palaeomagnetism

Palaeomagnetic studies of presumed Marinoan cap carbonates in Western Australia (Li 2000), Brazil (Trindade *et al.* 2003), and Oman (Kilner *et al.* 2005) have reported various patterns of geomagnetic reversal within directly-measured or composite lithostratigraphic sections. Limited rock-magnetic data and scanning electron microscope (SEM) imaging of Brazilian cap carbonates are interpreted to document detrital magnetite and detrital hematite as dual carriers of ancient magnetization (Font *et al.* 2005). The unexpectedly long duration of deposition that is seemingly required to account for numerous geomagnetic polarity reversals in cap carbonate calls into question most models of rapid Snowball deglaciation, or at least casts aspersion on the primary nature of those magnetizations or the interpretation of those rock magnetic data. This report details rock-magnetic and environmental-SEM petrographic analyses of iron-bearing phases contained in Nuccaleena Formation cap dolostone in order to establish hematite as the predicted primary character of that unit's magnetization.

Regional geology

Elatina–Nuccaleena contact may be traced along a nearly continuous outcrop belt north from

Bunyeroo Gorge, past the area of Trezona Bore, a distance of *c.* 20 km entirely within Flinders Ranges National Park in the vicinity of the Heysen Trail (Oraparinna 1:100 000 mapsheet; Wilpena 1:63 360 mapsheet; Flinders Ranges National Park mapsheet, Callen & Reid 1994). NW-, W-, and SW-dipping sections are best exposed in minor and major intermittent-stream drainages incising the neotectonically active (Celerier *et al.* 2005) western margin of Flinders Ranges. The strike of this belt is nearly parallel to the north–south trend of Torrens Hinge Zone, a post-Elatina structure roughly delineating the late Ediacaran depositional shoreline (Fig. 1). During Elatina glaciation, subaerial facies (Williams & Tonkin 1985) are preserved *c.* 70 km west of the modern location of Torrens Hinge Zone at the latitude of the outcrop belt of this paper, and submarine facies are also preserved west of the trace of Torrens Hinge Zone.

Sections detailed here are from Elatina Creek, Enorama Creek (Ediacaran GSSP), and composite from several ravinements draining easterly hills and plains close to the immediate southeast of Trezona Bore (Fig. 1, Table 1). The section at Trezona Bore was considered as an alternative candidate for the Ediacaran GSSP (discussion can be found in reports of the International Commission on Stratigraphy's Terminal Proterozoic Subcommission, at http://www.stratigraphy.org/precambrian/tptz.htm). The section at Elatina Creek is informally considered, and in this report formally suggested, as a parastratotype that is better suited than Enorama Creek for continuous exposure and scientific sampling (K. Anderson, N. Bailey, and J. Gehling, pers. comm. 2004).

With isopachs influenced by multiple episodes of rifting beginning *c.* 175 million years before deposition of Nuccaleena Formation and with migrating loci of prolonged diapirism influencing accommodation space, this central zone of the Adelaide Rift Complex does not follow simple rules of basin architecture (Lemon & Gostin 1990; Preiss 1990, 2000). Elatina Creek and Enorama Creek sections are roughly equidistant and distal to the main exposed body of Oraparinna diapir; Trezona Bore section is relatively proximal to the northern arm of Oraparinna diapir, termed, wholly or partly, 'Enorama diapir' in some publications, e.g. Lemon (2000) and Knoll *et al.* (2006) (Fig. 1).

Although Cambrian rifting and Cambrian-Ordovician intrusive orogenesis are restricted to southern and eastern Adelaide Rift Complex (eastern Mount Lofty Ranges) (Preiss 2000), cleavage and general indicators of that thermal event extend somewhat further from the locus of magmatism. However, the central Flinders zone has experienced only low-grade Phanerozoic regional metamorphism. The SE-dipping, frontal thrust associated with medium-grade Delamerian deformation is *c.* 50 km south of Elatina Creek section (Marshak & Flottman 1996). Although the northern and central Flinders zone may have experienced late Palaeozoic to Mesozoic block tectonism (folded Triassic coal measures are exposed at Leigh Creek to the north of the sections described, and near Quorn to the south), open folding in the central zone is considered syn- and shortly post-Cambrian in age. Gently dipping Mesozoic strata flank both margins of Flinders Ranges; these likely have been disturbed only by Cenozoic neotectonic deformation.

Lithostratigraphy

Enorama Creek, GSSP

Although Elatina Formation may be mapped in subcrop and float on the broad plain between Enorama Creek and Brachina Gorge road and geological trail, it is dominantly covered by streambed gravel and canyon-wall colluvium near to Enorama Creek. During numerous visits to the site, we have observed upper Elatina diamictite intervals emerge from and disappear beneath migrating boulders in the creek (Fig. 2a). These diamictite beds, which vary in matrix colour from moderate red 5R 4/6 to dark reddish brown 10R 3/4, include outsized boulders of quartzite, andesite, basalt, specularite, and granite in fine-grained matrix.

A singular exception is one bed which contains a *c.* 70 cm wide by *c.* 20 cm thick raft of yellow-weathering, planar-laminated pink sandstone (Fig. 2a). Lemon & Gostin (1990) invoke reworking of prior Elatina glacial deposits for most, if not all, deposition of upper Elatina diamictite and indeed, a similar sandstone bed crops out near the bottom of the Elatina section at Elatina Creek, some 4 km south of Enorama Creek. For this and other reasons, Elatina Formation diamictite provenance is generally considered, at least in part, locally sourced.

At least two metres of cobble-bearing, fine-grained, massive diamictite are probably perpetually exposed as a sloping creek wall closely below the Ediacaran GSSP. The diamictite appears less conglomeratic upward and undergoes a transition into a relatively resistant, coarse-grained, greyish red 10R 4/2, convolute-laminated, flaser-bedded arkose (hereafter, 'red sheet sandstone'). The red sheet sandstone is unquestionably distinct from, and erosive into, the immediately underlying massive siltstone, and at outcrop scale the loading surface is easily defined (Fig. 2a, b).

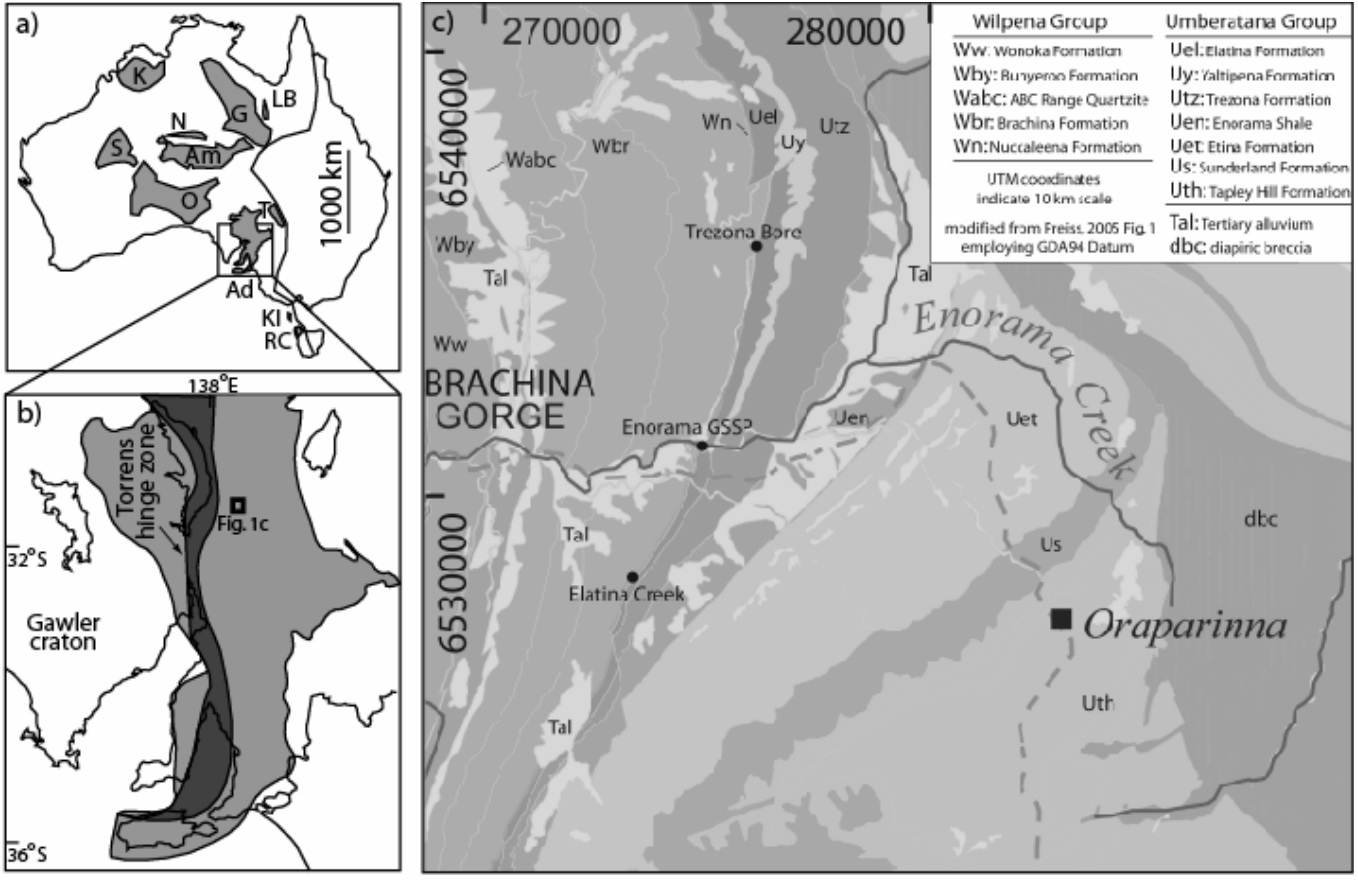

Fig. 1. Regional geology. Modified from the inset map of Preiss (2005), from 1:250 000 Parachilna geologic mapsheet. (**a**) Approximate outcrop limits of Australia's Neoproterozoic basinal blocks. K, Kimberley; S, Savory; N, Ngalia; Am, Amadeus; G, Georgina; LB, Little Burke outlier; O, Officer; Ad, Adelaide; T, Torrowangee; KI, King Island; RC, Rocky Cape; (**b**) Close-up of Adelaide Rift Complex, exposed in Flinders fold belt. Torrens hinge zone approximates the mid- to late-Ediacaran shoreline of the eastern edge of Gawler craton. (**c**) An *c.* 50 km_2 area of the central Flinders zone discussed in this report. Three sections at Elatina Creek, Enorama Creek, and near Trezona Bore expose Elatina–Nuccaleena contact with varying character. Oraparinna diapir and its northern arm (Enorama diapir) are inferred to be active during early Elatina time because of the corresponding isograds of its fringing reefs, including Trezona Formation to the west, and preservation of a locally-restricted, basal Elatina glacial unit in the same sink (Lemon & Gostin 1990; Sohl *et al.* 1999). All sites are in Flinders Ranges National Park. Access to Enorama Creek via public road and *c.* 200 m trail. Access to Elatina Creek via *c.* 2 km hike or gated park-service road. Access to Trezona Bore via *c.* 6 km hike or gated park-service road.

Table 1. *Sample information*

Site	Northing	Easting	Sample No.	Position	Technique	Details
Trezona Bore	6535080	276050	TBNU 28	Carbonate interbed in lower Brachina shale, *c.* 75 cm above base	Thermosusceptibility	Run 1: peak temperatures 321°C, 691°C Run 2: peak temperatures 459°C, 557°C, 584°C, 636°C, 673°C, 710°C
			TBlag1	Nuccaleena, basal *c.* 5 cm	eSEM	Not figured
Enorama Creek	6231050	274750	GSSP 31	Nuccaleena, 2.06 m above base	Thermosusceptibility	Run 1: peak temperatures 326°C, 490°C, 595°C, 711°C, 572°C, 595°C, 712°C
			GSSP 30	Nuccaleena, 1.7 m above base	Hysteresis	
Elatina Creek	6528200	273000	NUEL 131	Carbonate interbed in Brachina shale, 5.91 m above Nuccaleena base	IRM acquisition	
			NUEL 123	Nuccaleena, 4.16 m above base	IRM acquisition	
			NUEL 57	Nuccaleena, 1.98 m above base	eSEM	
			NUEL 16	Nuccaleena, 47 cm above base	Hysteresis	
			NUEL 148	Nuccaleena, 29 cm above base	IRM acquisition	
			NUEL 147	Nuccaleena, 25 cm above base	IRM acquisition	
Bunyeroo Creek	6522500	274000	SCN 4	Nuccaleena, 5.67 m above base	IRM acquisition	
			SCE 3	red sheet sandstone, 9.54 m below contact	IRM acquisition	

*Position to nearest 50 m, AGD84. eSEM (see Fig. 6). thermosusceptibility, hysteresis, IRM acquisition, (see Fig. 7).

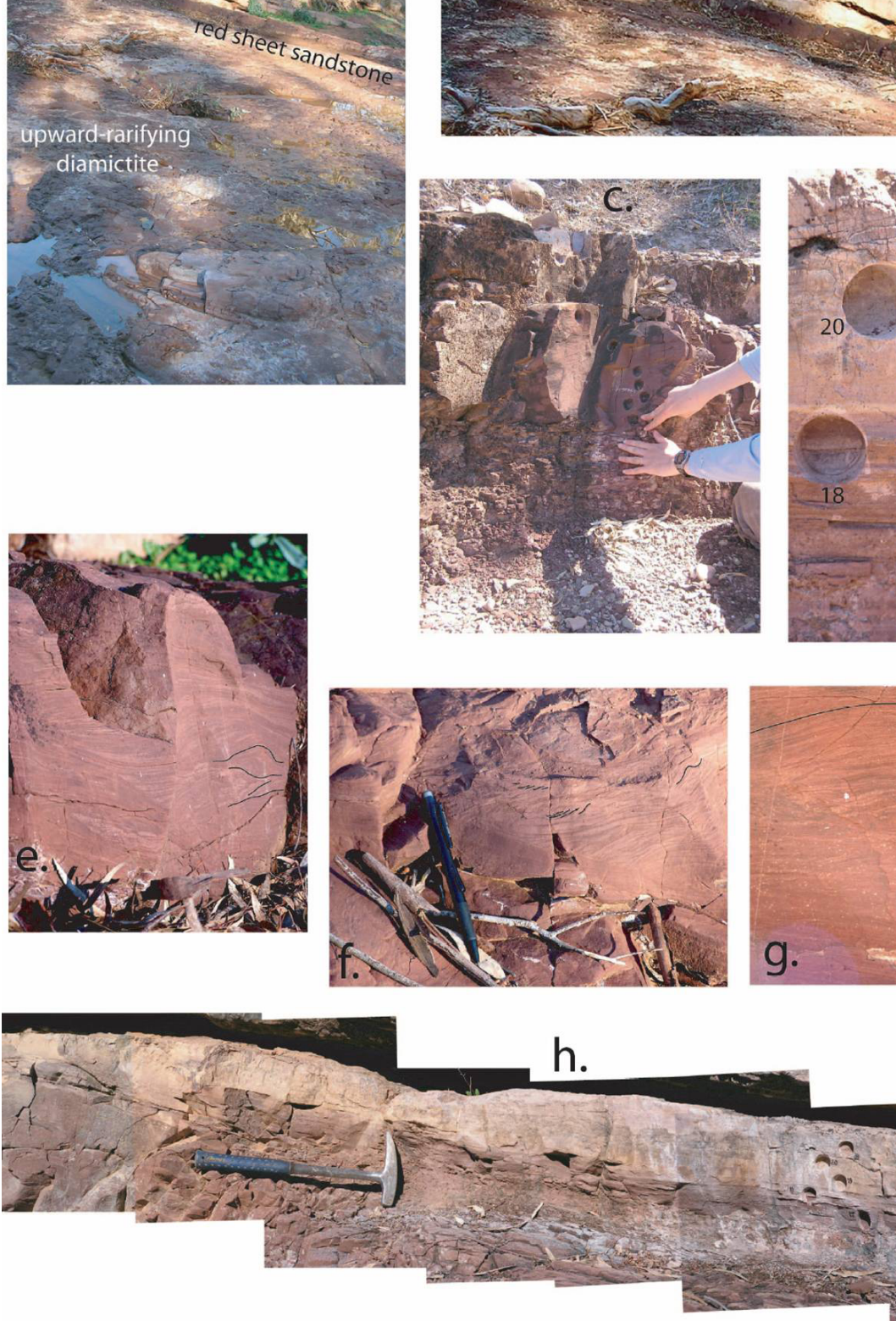

Fig. 2. Enorama Creek GSSP. Key facies and contact relations through Elatina-Nuccaleena tra
Enorama Creek GSSP. (**a**) Eastward view from the base of continuous exposure, 2003. Note pink
raft as diamictite clast in foreground. Diamictite becomes less conglomeratic upward, and is inc
sheet sandstone (resistant ledge, above label, beneath Nuccaleena hillside outcrop). Much of the f

However at hammer-scale, cleavage in the lower part of the sheet sandstone (later, reassigned to basal Nuccaleena Formation) and transposed nubbins weathering texture in the topmost siltstone of Elatina Formation interfere and often make precise placement of a contact difficult (Fig. 2c). Over a zone of several centimetres upward, however, cross- and convolute-bedded lamination (Fig. 2e, f, g) in the sheet sandstone disappears. Hypothesizing remaining, mean planar flaser fabric of the red sheet sandstone as palaeohorizontal, the unit could incise underlying massive diamictite by *c.* 46 cm, have *c.* 11 cm top-surface relief, and vary between *c.* 55 cm and *c.* 110 cm thick over an exposure scale of *c.* 4.8 m (Figs 2a, b).

In a detrital zircon study, Gehrels *et al.* (1996) dated fifty zircon crystals, presumably from this sheet sandstone unit and locality. Dominated by *c.* 1630–1570 Ma grains, the age spectrum of the Elatina red sheet sandstone could be sourced from the Nuyts volcanics and St Peters Suite, and the Hiltaba Suite, respectively, of adjacent Gawler Craton to the west. Alternative, east-derived sources from Curnamona Province or from southern Flinders inliers are also possible. If sourced from Gawler Craton, heavy mineral stringers throughout Elatina Formation might represent detrital input from Middleback Iron Formation, close to Torrens Hinge Zone and slightly south of due west from Enorama Creek. Noting contrast, then, with the mixed or local (diapir and underlying Elatina Formation) dominated provenance of Elatina diamictite, the depositional environment appears to have changed, at least itinerantly, across the uppermost Elatina diamictite to sheet sandstone transition to record locally voluminous input from continental sources.

Where bed top relief is greatest in the red sheet sandstone, near the creek bed, the unit encloses a laterally discontinuous, *c.* 6 cm thick mudstone lens and is depositionally overlain by similar, greyish brown 5R 3/2, rare pebble-bearing, rubbly-weathering mudstone. Multiple calcareous-weathering horizons laminate an uppermost, coarser, redder interval of the mudstone unit immediately beneath solid Nuccaleena Formation cap dolostone, which displays sharp, centimetric-undulatory contact with Elatina Formation (Fig. 2h here; fig. 5e of Lemon & Gostin 1990). These calcareous horizons are conservatively assumed to represent Nuccaleena-age diagenetic fronts invading topmost Elatina siltstone. Palaeomagnetic drill holes that are now partly obliterated by the GSSP golden spike demonstrated horizontal continuity and sharp margins of these layers into the outcrop (Fig. 2d).

Where red sheet sandstone is thickest, however, the rubbly mudstone, siltstone, and mixed-calcareous-weathering interval is attenuated or even unexpressed, and the solid Nuccaleena Formation cap dolostone closely overlies the red sheet sandstone, with a *c.* 1–10 cm re-entrant masking the contact (Fig. 2b). Chalky-weathering carbonate may be dug out of this crevasse, suggesting a correlation with the mixed-calcareous-weathering interval exposed further down the creek slope. Even so, the thickness of calcareous-weathering siltstone filling relief atop the red sheet sandstone appears to vary by a factor of *c.* 2 across the span of exposure (see schematic lithostratigraphic sections and sequence-stratigraphic summary, Fig. 3).

Bed 1 of solid Nuccaleena Formation cap dolostone at Enorama Creek is recrystallized and undulose at low amplitude. Centimetric, spar-filled sheet cracks are common. Ensuing beds are buff-weathering (greyish orange 10 TR 7/4), pale red

Fig. 2. (*Continued*) evident near the site of dramatic downcutting of the red sheet sandstone, in the sandstone, the underlying diamictite, or in the smooth-weathered units occupying the re-entrant, when viewed with a flashlight. (**c**) Lower contact of red sheet sandstone into non-conglomeratic Elatina siltstone. While sandstone cleavage tends to interfere with loading-induced nubbins weathering-style of underlying siltstone, presence/absence of heavy-mineral lamination is the useful diagnostic. Contact between left thumb and right forefinger. Palaeomagnetic samples drilled in both units. (**d**) The Basal Ediacaran GSSP 'Golden Spike' interval. Samples #17–21 of TDR's collection. Formal placement of the Cryogenian–Ediacaran Period 'unconformity' between samples 20 and 21. Note three-dimensional, sharply defined, calcareous-weathering horizons extending downward, even into sample 17. While interpretation as post-depositional diagenetic fronts is plausible and conservative here at Enorama Creek, similar features are undeniably primary sedimentary just *c.* 2 km to the south, at Elatina Creek. (**e**) Undulose to planar-lamination surrounding disrupted (bifurcated) lamination at lower right, in red sheet sandstone unit. Bordering construction lines. (**f**) Climbing and starved ripples amidst otherwise planar-laminated flaser-bedded siltstone. Change in attitude of exposure across line from upper left to lower right. (**g**) Convolute bedding includes overturned laminae and near-vertical exposure. Altogether, indications in the red sheet sandstone range from high to low flow regime, and appear to permit both sudden depositional episodes and prolonged deposition. Though strange in the context of Enorama Creek alone, these different aspects are sensible in context of similar units at Trezona Bore to the north and Elatina Creek to the south. (**h**) Elatina–Nuccaleena contact just before it disappears into re-entrant. Note attenuation of supra-red sheet sandstone calcareous-weathering mudstone-and-siltstone unit upward and to the left.

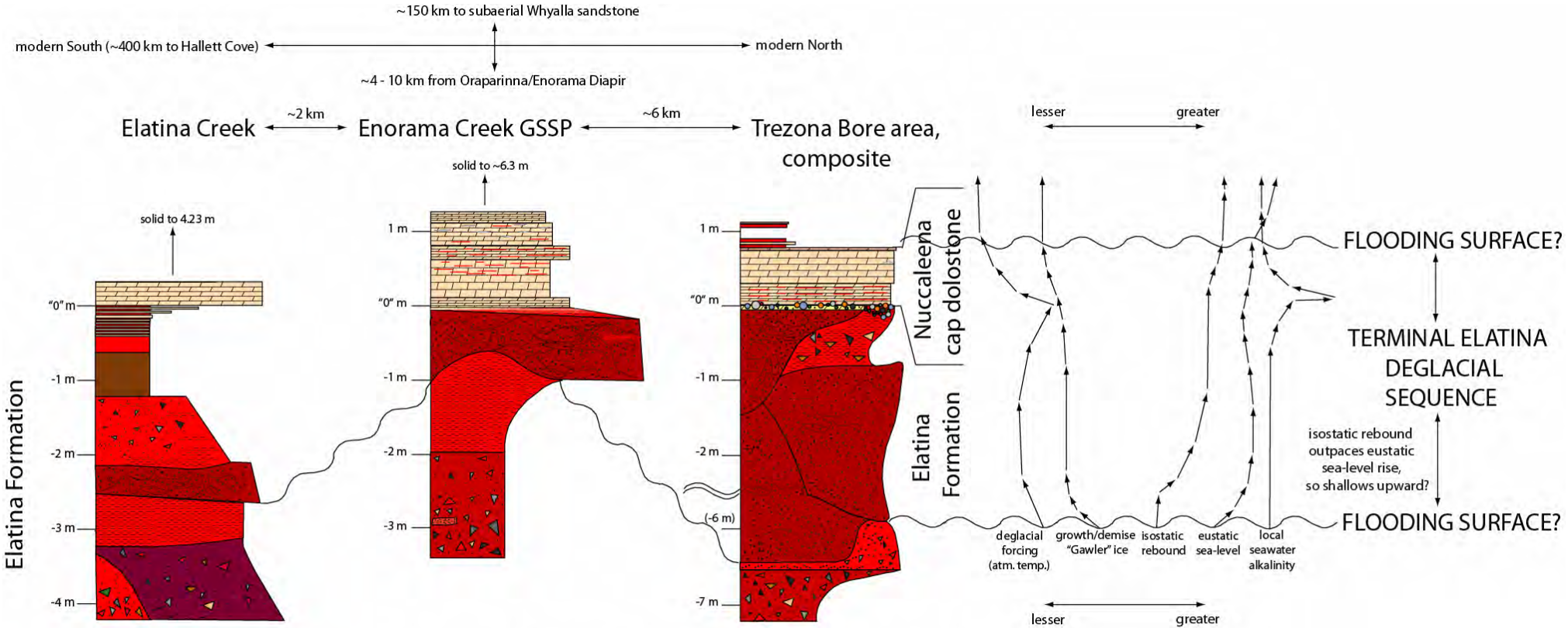

Fig. 3. Nuccaleena Formation Terminal Elatina Deglacial Correlation Scheme. Schematic lithostratigraphic profiles of Elatina–Nuccaleena transition intervals at Elatina Creek, Enorama Creek, and in the Trezona Bore area. Note that at Trezona Bore, only profiles on the right and left sides of the cartoon section are directly observed. All other relations are inferred or required by the observation that all sections in the area possess at least one red sheet sandstone bed (some expose three nested sandstones) and both sections examined in detail possess a basal Nuccaleena lag, assumed to represent a locally persistent time-horizon, possibly an exposure or a flooding surface. Five physical variables probably sufficient to model predicted litho/sequence-stratigraphic outcomes of Elatina deglaciation are listed, with highly speculative senses of growth/diminution. It is not clear whether solid Nuccaleena Formation cap dolostone deepened or shallowed through its interval of deposition. Though conventionally regarded as a flooding-surface at the base of a transgressive system tract, onset of Nuccaleena Formation cap dolostone may reflect some nontrivial combination of senses of change in these five variables, or of interaction with a dynamic chemocline (Hoffman 2005). We preserve the notion of basal Nuccaleena flooding by appealing to isostatic rebound to dominate the siliciclastic portion of the terminal Elatina deglacial sequence, and eustatic sea level rise to dominate the carbonate portion. Alternative explanations are suggested in the text.

10 R 6/2-coloured, medium-fine grained, low-angle cross-laminated peloidal dolomicrites. The abundance of sheet cracks (thin, discontinuous red silt horizons, and oversteepened, centimetric peloidal antiforms) decreases upsection. Outcrop-scale stylolite horizons of low tortuosity are episodic throughout the *c.* 5.8 m of Nuccaleena Formation cap dolostone exposed at Enorama Creek (total thickness *c.* 6.3 m, with an obscure interval disrupted by the root system of a large eucalyptus tree). These might reflect Delamerian attenuation of the section; however they could also mark primary or early diagenetic dissolution surfaces.

Full lithostratigraphy of Nuccaleena Formation cap dolostone is left for future description; this report focuses on the Elatina-Nuccaleena contact interval (except where basic description of stratigraphically-higher Nuccaleena Formation cap dolostone is appropriate to provide context for rock magnetic results).

Elatina Creek

While Elatina Creek section of Elatina Formation is potentially attenuated by faulting mid-unit, the upper portion is coherent (Fig. 4a). Fine-matrix, massive red diamictite indistinguishable from the lowest unit described above at Enorama Creek hosts outsized boulders and is incised by dark reddish brown 10 R 3/4, medium-grained, matrix-supported, cobble-bearing channelized diamictite, in turn topped by pebble- to cobble-bearing, fine-grained, massive diamictite. A red sheet sandstone unit (Fig. 4a), ranging from *c.* 37 cm to >50 cm thick, incises conglomeratic Elatina Formation by at least *c.* 3 cm over an outcrop scale of *c.* 6 m (small-scale faults cut the unit and make determination of incision relief somewhat ambiguous). The sheet sandstone does preserve at least 10 cm of relief on its top surface, in which red, laminated siltstone is preserved and presumed to mark palaeohorizontal.

Although the flaser-bedding is not as apparent at Elatina Creek as at Enorama Creek, this unit is continuously traceable (excepting intermittent alluvial cover) for *c.* 2 km north to Enorama Creek and likely reflects the same depositional era as the zircon-bearing red sheet sandstone unit described in the previous subsection. The same lithology appears *c.* 6 km north of Enorama Creek (next subsection), and later we suggest the base of this red sheet sandstone unit, best exposed at Elatina Creek, marks a regionally-extensive sequence boundary extending upward through ultimate deglaciation of the Elatina Snowball ice age.

At Elatina Creek, the red sheet sandstone unit is depositionally overlain by *c.* 60 cm of fine-grained, sparse pebble-conglomerate, which grades into *c.* 80 cm of rubbly-weathering, non-conglomeratic mudstone. Unique among sections we have observed in Flinders Ranges, Elatina Creek section exposes a continuous stratigraphic profile across the Elaina-Nuccaleena transition, and it is strikingly conformable (Fig. 3). Within *c.* 55 cm of solid Nuccaleena Formation cap dolostone, rubbly-weathering, non-conglomeratic mudstone begins to pick up coarser siliciclastic grains and becomes increasingly laminated, presenting a calcareous weathering profile mixed at centimetre-scale with intermittent, fine-grained siliciclastics.

Within decimetres of the contact, these mixed units gain lateral persistence and display unequivocal loading structures: red silt flames asymmetrically downward into calcareous-weathering, buff silt (Fig. 4b, d). This relation seems consistent with depositional origin as centimetric siliciclastic debris flows overriding unconsolidated, partly calcareous ooze. In this framework, palaeocurrents would have been generally toward either the NE or SW (asymmetric structures verge both directions). Although the calcareous-weathering beds only rarely yield identifiable primary carbonate petrographic textures, the density distinction evident in the inverted flame outcrop texture of some calcareous-siliciclastic doublets requires distinct bulk sedimentary compositions.

Fraction of calcareous-weathering lithology increases dramatically upward, and calcareous beds become compositionally unequivocal within *c.* 22 cm of the basal Nuccaleena contact, especially at creek level, where at least two beds of carbonate interfinger with red siltstone (Fig. 4c) preceding outcrop of recrystallized carbonate in 'bed 1' of Nuccaleena Formation cap dolostone. Continuous exposure may be dug out of the creek bed, and both *c.* 3 cm thick carbonate beds are sharply surrounded by unbroken red siltstone.

As at Enorama Creek GSSP, bed 2 and all ensuing beds in the *c.* 4.2 m thick, continuous outcrop of Nuccaleena Formation cap dolostone are cross-laminated at low-angle, comprising submillimetre to *c.* 2 mm peloids generally evident in weathered outcrop but rarely in thin-section, and sometimes inversely graded. Spar-filled sheet cracks and centimetric, oversteepened, sharp-crested peloidal antiforms are present in the lower part of the section.

Laterally extensive and vertically continuous, fresh exposure of uppermost Elatina Formation and most of Nuccaleena Formation at Elatina Creek renders this site as an exceptional section for study of the GSSP interval. Precise placement of the GSSP is nontrivial since, in contrast with the section at Enorama Creek, the basal Nuccaleena contact at Elatina Creek is convincingly conformable. In spirit, the Ediacaran Period at Elatina

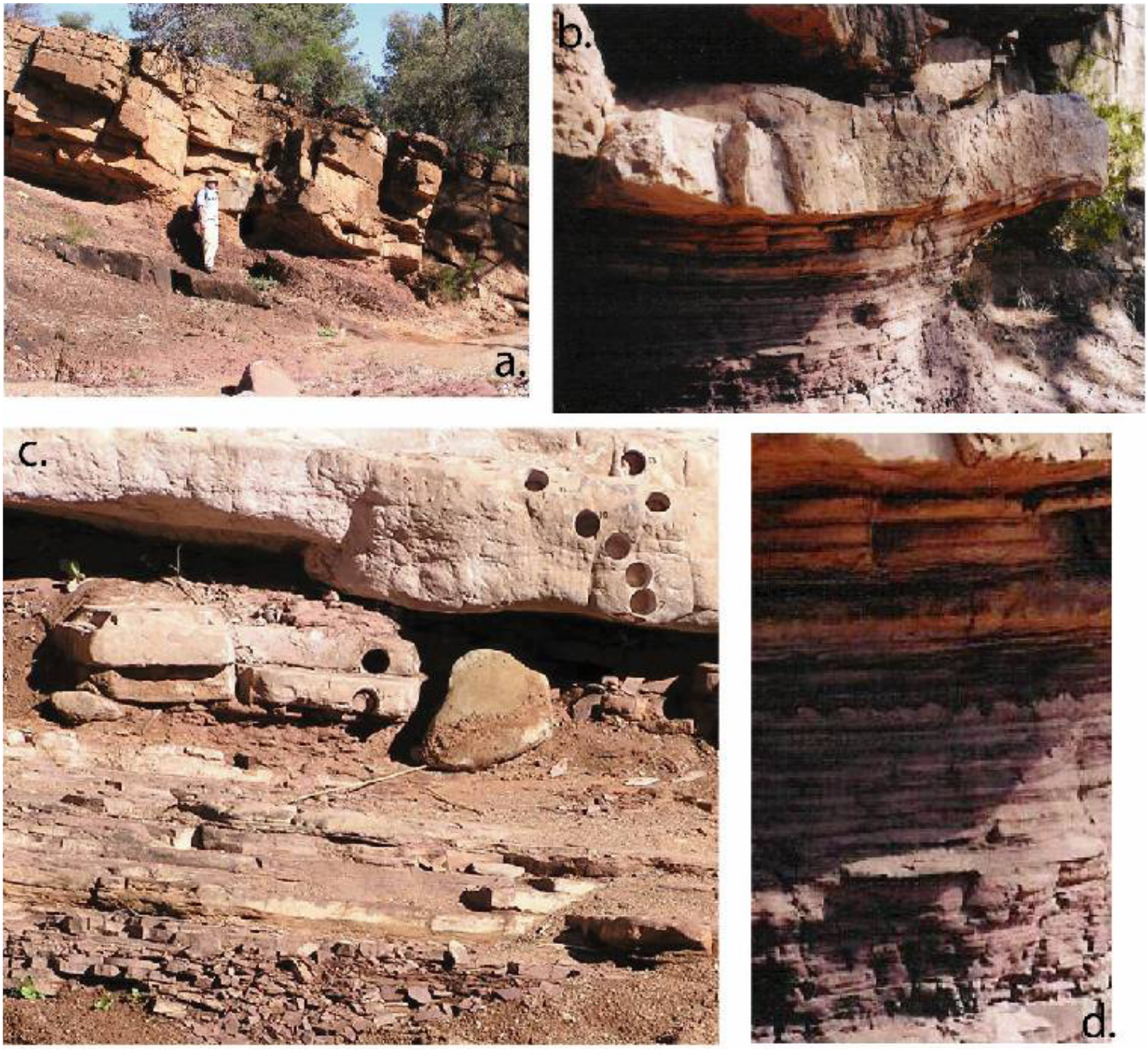

Fig. 4. Elatina Creek. (**a**) Cliffy exposure of proposed Ediacaran parastratotype. Creek runs left to right in foreground. Geologist Ryan Petterson, *c.* 1.8 m, for scale, standing on top surface of red sheet sandstone. (**b**) Mixed siliciclastic-carbonate interval of deglacial sequence, here assigned to lower Nuccaleena Formation. Carbonate-in just below shadow inflection; undulose current-loading of siltstone onto carbonate (ooze?) most prominent in middle bed. Two of the three topmost carbonate beds, separated by fine layers of siltstone, are present in creek bed, *c.* 5 m to right. They clearly underlie disrupted carbonate forming a 'keystone' block in bed 1, associated with a strange 'tepoid' structure, above shadow at head level in (a). (**c**) Creek bed exposure of the simplest-correlated 'GSSP' level, at the base of solid carbonate bed 1 (nearly continuous exposure in re-entrant visible with a flashlight). (**d**) Close-up, Elatina–Nuccaleena transition.

Fig. 5. Trezona Bore area. (**a**) Multiple sets of presumably glacial striations on a diapir-derived (?) basic volcanic clast above red sheet sandstone and highest successful palaeomagnetic site of Sohl *et al.* (1999), in sparse diamictite interval below cover including subcrop of cap carbonate. (**b**) *c.* 75 cm highly-weathered Nuccaleena Formation cap dolostone dug out of cover at top of Sohl *et al.*'s magnetostratigraphic section. The carbonate sits directly atop a grit-to-pebble layer, which sits above non-conglomeratic siltstone (only *c.* 8 cm dug out). (**c**) Best-exposed Nuccaleena section in area, up hillside gully to north of Sohl *et al.*'s (1999) section. (**d**) Full thickness of cap carbonate at magnetostratigraphic section, note spackly-weathering micrite layer at top, and thinner analogues lower in section. (**e**) Close-up of spackly-weathering micrite v. low-angle cross-bedded peloidal dolomicrite. Apparent foresets in middle of view, below level of label. (**f**) Loose block, up-ended, exposes Nuccaleena Formation cap dolostone cementation of supra-red sheet sandstone pebble lag. The same basal cap carbonate lag lies *c.* 2 m higher than the top of a single red, sheet sandstone bed at Sohl *et al.*'s (1999) section, close to the south.

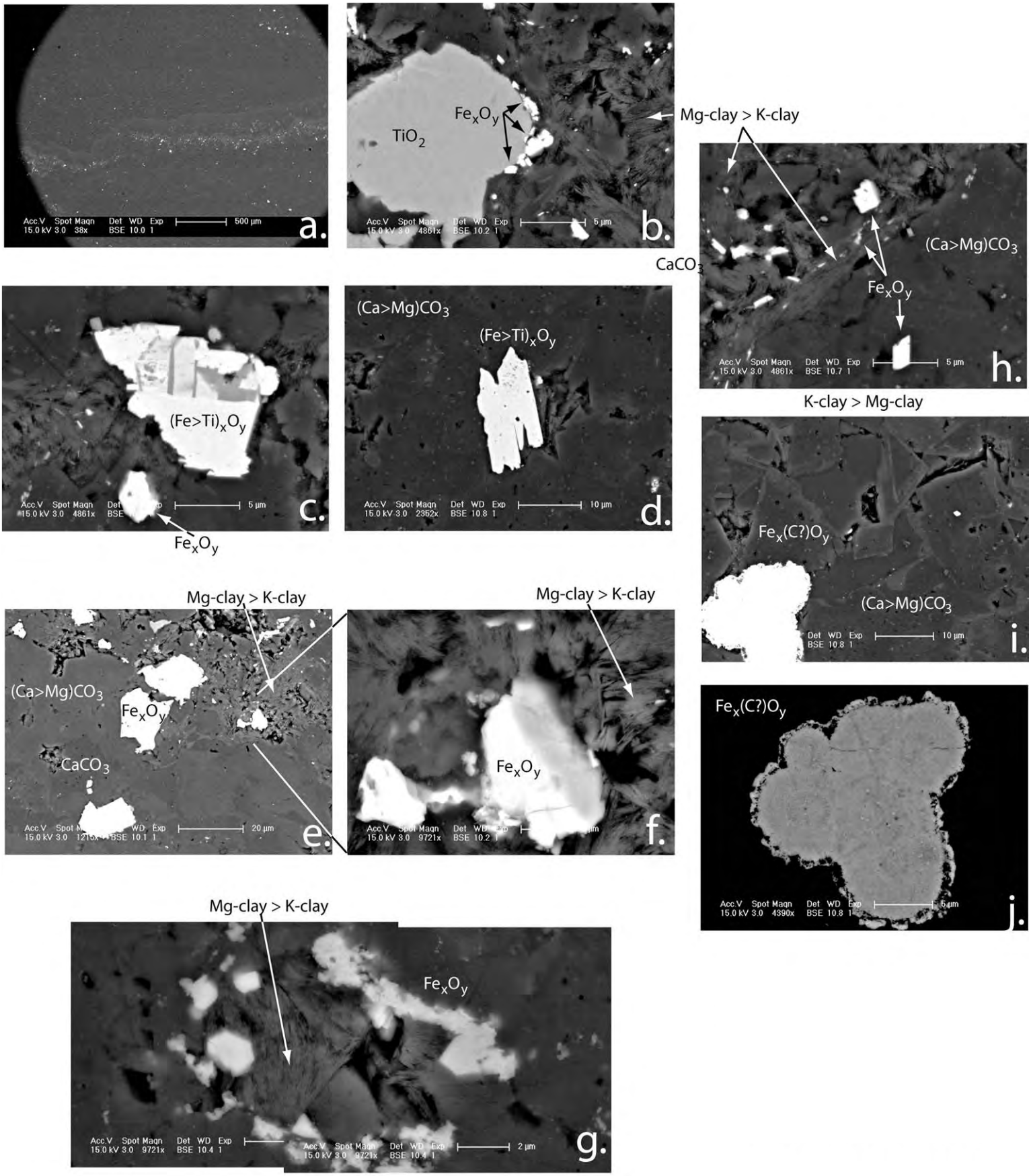

Fig. 6. eSEM petrography of terrigenous and carbonate cap constituents. Stratigraphic up is topward in all. Qualitative chemistry by EDS analysis, spectra not shown. (**a**) Heavy minerals often concentrated in undulose, subhorizontal layers, but also dispersed throughout carbonate-dominated portions of specimen. (**b**) Sub-micron iron oxide agglomerates clustered on clay-ward rim of rutile grain. Carbonate encroaches close to the other sides of this rutile. (**c**) Large, chemically zoned, Ti-bearing iron oxide; smaller iron oxide; and very small (EDS-unresolvable) iron oxide crystals near clay floc, sandwiched between dolomite crystal networks. (**d**) Platy Ti-bearing iron oxide adjacent to small pocket of clay, otherwise isolated in region of dolomite rhombs. (**e**) Irregular iron oxide grains and clay sector amidst mixed Mg-rich and Mg-poor dolomite, and calcite rhombs. (**f**) Magnified sector of e. (**g**) Clusters of putatively single domain-sized iron oxide crystals surrounding clay floc, in otherwise carbonate-dominated sector. (**h**) Smallest iron oxides appear to follow fabric of clay floc. (i) and (**j**) Single occurrence of botryoidal iron oxide (?). Preferred interpretation as a relict, microbially bound macropeloid/macro-ooid, with bio-induced rim precipitate. Since specimen was carbon-coated, it is possible the relict mineral is siderite or iron (oxyhydr)oxide.

Trezona Bore

About 6 km north of Enorama Creek, along a continuous but progressively shallowing homocline, the Heysen trail and an associated, gate-accessed 4WD track reach Trezona Bore amid mixed Brachina Formation sandstones and siltstones. Gentle undulation of regional folds shallows the westward dip of units to the east of Trezona Bore, so that Elatina and Nuccaleena formations are exposed mostly as dip-slope geomorphology and occasionally in creek cross-section over several kilometres to the south along strike. The Terminal Proterozoic Subcommission considered Trezona Bore as well as Enorma Creek and a third section, outside Flinders Ranges National Park as candidate GSSP locations (Knoll *et al.* 2006).

Sohl *et al.* (1999) report the best-constrained magnetostratigraphy of Elatina Formation from one of these creek sections, containing at least six reversals defined between sites that are separated by decimetres to metres of stratigraphic height. Noting the site-based sampling strategy employed and the regional heterogeneity and impersistence of glacial lithofacies, Sohl *et al.* (1999) stipulate 'six' as a minimum estimate for the number of geomagnetic reversals spanning Elatina deposition.

The topmost polarity zone in the Trezona Bore area section of Sohl *et al.* (1999) preserves a NE, shallow-down palaeomagnetic remanence direction; it is represented by two sites within a *c.* 2 m thick, red, sheet sandstone bed. Atop this bed, striated cobble-bearing, massive diamictite is poorly exposed (Fig. 5a), and *c.* 1 m higher, *c.* 10 cm of peloidal dolostone crops out of shale-fragmentary regolith. It is possible to excavate the regolith to a depth of *c.* 50 cm, which exposes a full thickness of *c.* 75 centimetres of shallowly-dipping cap carbonate sitting directly atop a poorly-consolidated pebble gravel (Fig. 5b), underlain *in-situ* by red, non-conglomeratic siltstone.

The Nuccaleena Formation cap dolostone outcrop disappears beneath fragmentary shale regolith along strike to the east. The resistant red sandstone in uppermost Elatina Formation, however, is readily traceable for a kilometre to the south and some distance, uphill, to the north and east. Over this distance, some dozen creeks expose it in profile; and variously one, two, or three distinct, red sheet sandstones are nested, with occasionally high-amplitude erosive contact.

The lithostratigraphic section figured from the Trezona Bore area (Fig. 3) includes not only the units atop Sohl *et al.*'s (1999) Elatina Formation magnetostratigraphy, but also a composite from sections in the deepest five creek beds south of that and (with digital pictures, Fig. 5) a section along a steep gully dissecting the backside of a hill only *c.* 400 m south of Trezona Bore. That creek cuts, at elevation *c.* 440 m, abruptly downward through Nuccaleena Formation cap dolostone (which is exposed in profile along strike over tens of metres and for about 1 m as clean, top-surface dip slope, due to the high topographic relief against easily-weathered, overlying Brachina siltstones).

Here, as immediately above the magnetostratigraphic section of Sohl *et al.* (1999), the solid Nuccaleena Formation cap dolostone is *c.* 75 cms thick (Fig. 5c). It is entirely peloidal cross-laminated except in its bottom *c.* 3 cm, in which carbonate of enigmatic origin cements a pebble to cobble-sized, heterolithic gravel lag sitting atop red sheet sandstone (Fig. 5d). Although eroded to a re-entrant at immediate creek level, vantage may be gained into the recess, and it is clear that the pebbles contained in basal Nuccaleena Formation cap dolostone directly load atop red sheet sandstone, the section lacking any intervening silt.

This is a basal disconformity to the letter of formal Ediacaran GSSP definition. Solid Nuccaleena Formation cap dolostone is essentially unbroken by thin siltstone horizons, in contrast to the sections at Elatina and Enorama creeks. A prominent spar-filled sheet crack occurs *c.* 50 cm above dolostone base (Fig. 5e); and solid carbonate is terminated by a *c.* 2 cm thick, non-peloidal-expressing, spackly-weathering bed of micrite (Fig. 5f). Two similar, but thinner, apparently micritic beds punctuate the solid dolostone near its half-thickness and toward its top (Fig. 5c, e). At least two more, thin, micritic carbonate beds are mixed with dominant siltstone in the ensuing *c.* 1 m, below continuous outcrop of Brachina Formation siliciclastics.

Downward in this gully from the Elatina–Nuccaleena contact, two red sandstone units are present; the higher incises the lower by at least *c.* 2 m on an outcrop scale. The bottom contact of the lower sheet sandstone unit cuts fine-matrix, heterolithic, boulder diamictite, which is the lowest traceable Elatina unit before outcrop disappears beneath alluvium.

We suspect, then, that the red sheet sandstone unit discussed at length in the Elatina Creek and Enorama Creek subsections represents multiple events of deposition, or else multiple events of erosion punctuating prolonged deposition of clastic, monolithic debris. Alternatively, a single red sheet sandstone bed might be deposited catastrophically, as during a jökulhlaup sourced beneath a waning Elatina ice sheet on Gawler Craton; and each section received detritus from a different number of such events. Preiss (2000), however, questions whether there ever was a low-altitude, continental ice sheet on Gawler Craton during Marinoan time.

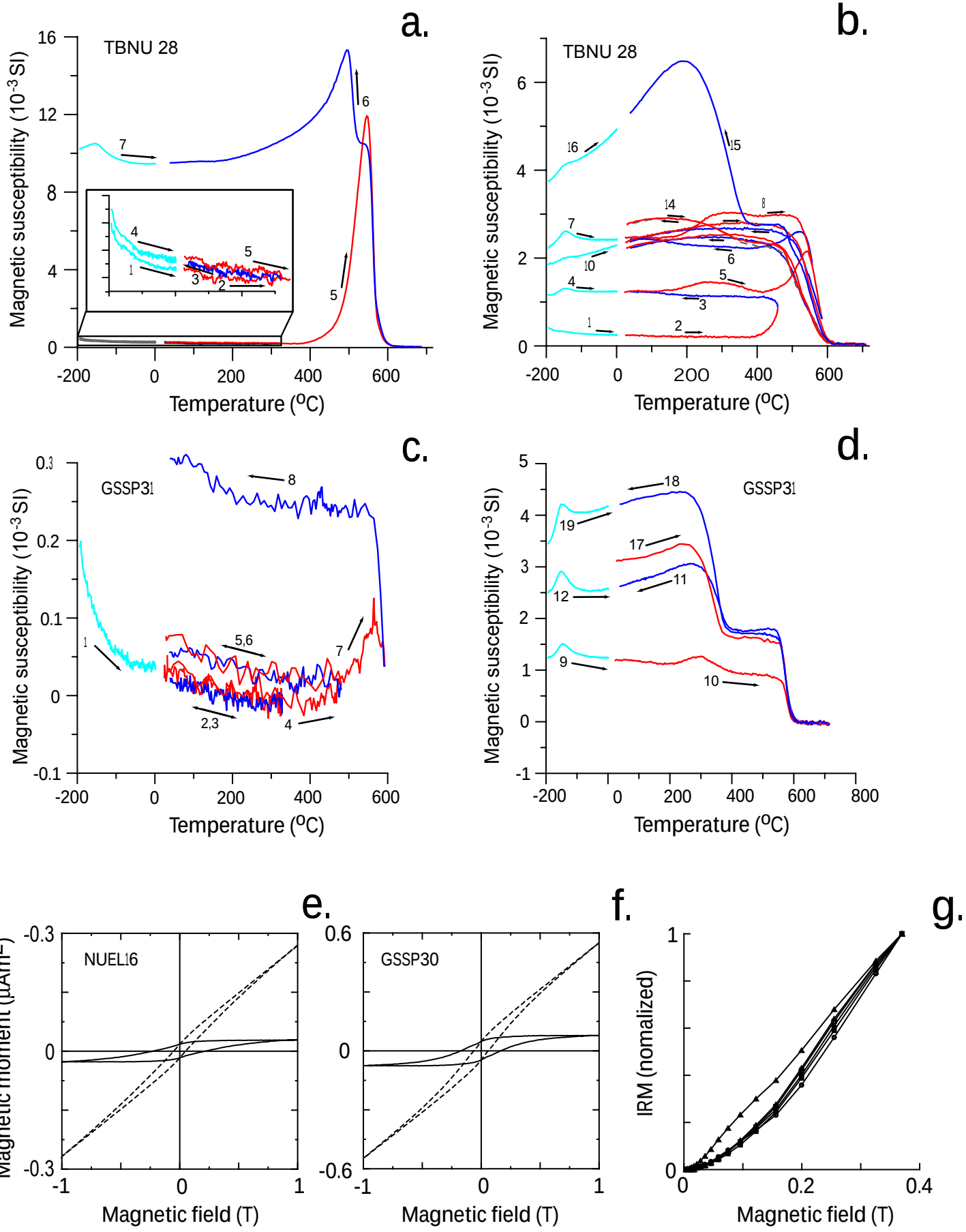
a.
TBNU 28
Magnetic susceptibility (10-3 SI)
Temperature (oC)
b.
TBNU 28
Magnetic susceptibility (10-3 SI)
Temperature (oC)
c.
GSSP31
Magnetic susceptibility (10-3 SI)
Temperature (oC)
d.
GSSP31
Magnetic susceptibility (10-3 SI)
Temperature (oC)
e.
NUEL16
GSSP30
Magnetic moment (μAm2)
Magnetic field (T)
f.
IRM (nomalized)
Magnetic field (T)
g.

Certainly, only two red sheet sandstone intervals are nested in the Trezona Bore gully, while up to three are expressed in west-draining creeks *c.* 800 m to the south, and four may be recorded atop a nearby summit to the north. Only one event (or uninterrupted interval of sheet sand deposition) is evident at Elatina Creek, while the mudstone enclave within the red sheet sandstone at Enorama Creek could permissibly argue for two events, or a sand hiatus within one prolonged depositional interval.

Summary

In a salt-withdrawal syncline actively accommodating sediment load in the central Flinders zone during Elatina glaciation, the Nuccaleena cap dolostone at Elatina Creek shows mixed conformable contact with underlying non-conglomeratic siltstones traditionally assigned to Elatina Formation. The nearest unconformable surface lies metres below the base of solid cap dolostone, beneath a thin interval of flaser-bedded, red sandstone. Along strike to the north, an identical lithofacies incises massive Elatina Formation diamictite at Enorama Creek GSSP, and is closely overlain by Nuccaleena Formation cap dolostone, with an intervening, thin interval of variable calcareous-weathering, non-conglomeratic siltstone. Still further north along strike, anomalously thin Nuccaleena Formation cap dolostone near Trezona Bore cements a gravel lag sitting variably above mostly non-conglomeratic siltstone or flaser-bedded, red sandstone. The 'red sheet sandstone' lithofacies near Trezona Bore consists of multiple depositional episodes, and at least three beds are nested, with occasionally high amplitude basal relief, sometimes bracketing pockets of bedded or massive diamictite. The base of the lowest red sheet sandstone closely beneath cap dolostone most accurately represents the basal Nuccaleena Formation (and Wilpena Group) sequence boundary.

Sedimentological interpretation

Our preferred interpretation of the uppermost Elatina-Nuccaleena package begins with Elatina boulder-diamictite sedimentation. This might define an era of net glacial advance (potential stadial/interstadial cycles aside); it might represent syn-Snowball sedimentation, if specific global climate dynamism were assumed or permitted at Elatina palaeolatitude (e.g. Warren *et al.* 2002; Goodman & Pierrehumbert 2003; Pollard & Kasting 2005); or it might represent a prolonged era of net glacial retreat (Lemon & Gostin 1990; Preiss *et al.* 1998), possibly associated with sea ice-bound oases occupying tropical embayments in the early stages of global deglaciation (Halverson *et al.* 2004). There is no easy intersection of the simple Snowball Earth theory with the timescale implied for mixed diamictic/nonconglomeratic siliciclastic deposition by six geomagnetic reversals (Sohl *et al.* 1999); but various authors have shown that the boundary conditions and dynamics of both hard and soft Snowball worlds are sufficiently malleable that neither hypothesis need seem disproved on the basis of those reversals alone (e.g. Pierrehumbert 2005; Pollard & Kasting 2005; and see Hoffman & Schrag 1998). A comprehensive sequence-stratigraphic framework for Elatina Formation remains elusive (despite preliminary suggestions of such a scheme in, e.g. Preiss *et al.* 1998), so all possibilities are currently permitted.

Nuccaleena Formation cap dolostone is not similarly permissive. Absence of dropstones in Nuccaleena Formation cap dolostone requires absence of ice-rafted debris and implies considerable waning, if not total disappearance, of tropical (whether or not Gawler Craton) ice sheets and/or (i.e. Adelaide Rift Complex) ice shelves. All other Nuccaleena inferences are, to date, model-dependent. For instance, major antiformal structures of enigmatic origin have been hypothesized as mega-teepee's (James *et al.* 2001), which could indicate exposure towards upper Nuccaleena Formation cap dolostone (Plummer 1979; Williams 1979). The same features might be referable to the 'megaripple' hypothesis (Allen & Hoffman 2005) developed for other Australian and Laurentian cap carbonates, and interpreted to require deep water. Mixed, variable transition of Nuccaleena Formation cap dolostone into Brachina shale is generally considered as a high stand systems tract, in part by assuming the presence or absence of laminated ribbon carbonates is controlled by carbonate compensation depth (e.g. Kennedy 1996).

In the rock magnetics section below, we note that Nuccaleena Formation cap dolostone pervasively contains terrigenous debris, especially detrital (titano)hematite and rutile, potassic and magnesium clays, and quartz, even in intervals macroscopically free of silt horizons. It is not clear whether trace apatite (not figured) is of detrital or diagenetic origin. Nuccaleena Formation cap dolostone seems, then, not to necessarily represent background flux of alkalinity otherwise suppressed by siliciclastic input (for one relevant discussion of mixed shale and carbonate sedimentation, see Chetel *et al.* (2005). Instead, we favour Nuccaleena Formation cap dolostone marking overwhelming flux of alkalinity introduced *de novo* near its base and waning gradually near its top (where calcite compensation depth (CCD) may certainly have effect). Shale input to the Adelaidean depocentre

may have been shut down during Nuccaleena deposition—or at least diminished during lower Nuccaleena deposition and disappeared during upper Nuccaleena deposition—or alternatively, deposition rate of Nuccaleena Formation cap dolostone might be so high as to dominate normal shale input in the lower half of the unit, and swamp it outright in its upper interval.

Regardless, it is stressed that the influx of alkalinity to the Adelaidean depocentre cannot represent initial sedimentation accompanying onset of terminal deglaciation. Elatina Creek preserves silt turbidites encroaching on incipient carbonate oozes at the beginning of Nuccaleena age. These silt turbidites are the energetic gradational superiors to rubbly mudstone that filled palaeorelief atop sheet sand beds marking (episodic or protracted) influx of coarse debris from Gawler Craton. The erosional event that preceded or accompanied initial deposition of these red sheet sands marks the oldest recognizable boundary delimiting a terminal deglacial sequence (widely regarded as a transgressive system tract) including Nuccaleena Formation cap dolostone from earlier, possibly pre- or syn-Elatina glacial deposits (Fig. 3).

This scheme seems to account for the Trezona Bore area disconformity expressed by a gravel lag atop red sheet sandstone and calcified by basal Nuccaleena Formation cap dolostone only if the siliciclastic portion of the Elatina–Nuccaleena terminal deglacial sequence were confined to an era of post-glacial isostatic rebound outpacing glacio-eustatic sea-level rise. Since Elatina red sheet sandstone is non-conglomeratic, the lag must be a post-sheet sand depositional event. The lag sits directly atop the second of two sheet sands in our Trezona Bore section but atop poorly conglomeratic siltstone filling red sheet sandstone palaeorelief at the Sohl *et al.* (1999) Trezona Bore section. It conveniently, therefore, might represent melt water-emplaced debris derived locally from northern Oraparinna/Enorama diapir, largely winnowed and deflated by diapir rebound (during the era of uppermost Elatina mixed siltstone-carbonate and/or lowermost Nuccaleena deposition, prior to transgression during lower or upper Nuccaleena time).

Finally, we note non-unique coherence of our model with some published interpretations of the presumed Nuccaleena-correlative carbonate unit in the Marinoan type section at Hallett Cove, south of Adelaide. Here, non-conglomeratic 'Seacliff' sandstone overlies the basal Wilpena Group sequence boundary and spans a thick stratigraphic interval between sparsely conglomeratic beds and a several metre-thick interval of mixed dolostone and siliciclastics (e.g. Christie-Blick *et al.* 1995).

Along the length of the Torrens Hinge Zone, Seacliff sandstone occupies various positions and displays various compositions (Preiss 1993), so its presentation at Hallett Cove should not be taken as generally representative. At Hallett Cove, however, the first appearance of cap carbonate is as decimetre-scale beds with purportedly concordant lower contacts but reworked top surfaces (unpublished theses of E. M. Alexander and I. A. Dyson; e.g. citation of the former in Lemon & Gostin 1990). Sandstone between these interbeds is hummocky cross-stratified and presumably responsible for high-energy scouring of each thin carbonate interbed (Dyson 1992). Only the highest carbonate bed, *c.* 1 m thick, is uninterrupted and unscoured at its top.

Although Hallett Cove is sufficiently distant from the central Flinders zone to permit several model-driven relative age relations between Nuccaleena outcrops of the two areas, simple lithostratigraphic correlation is now possible by considering the Elatina Creek section. The Hallett Cove mixed carbonate-siliciclastic interval is certainly more clearly expressed than at Elatina Creek, and it is thicker (*c.* 6 m versus *c.* 55 cm). Solid, overlying cap carbonate at Hallett Cove is, however, attenuated relative to Elatina Creek (*c.* 1 m v. 4.2 m). Accepting the widespread assumption that top-Nuccaleena transition to ribbon carbonate is CCD-controlled amid a high stand systems tract, Hallett Cove must occupy a deeper-water setting than Elatina Creek, if deposition rates of solid carbonate are broadly similar.

This is plausible given Elatina Creek's proximity to presumed-emergent Oraparinna diapir, and several consequences seem implied by accepting the water-depth interpretation of the preceding paragraph. First, expansion of the Hallett Cove sub-cap mixed interval over the same interval at Elatina Creek would appear to favour upwelling rather than surface origin for cap-controlling alkalinity, if mixed siliciclastic-carbonate deposition rate is approximately equal at the two locations. Upwelling origin of alkalinity for cap carbonates (Grotzinger & Knoll 1995) is not simply compatible with interpretations of other aspects of cap carbonate sedimentology (Higgins & Schrag 2003; Shields 2005); but when considered in isolation of those arguments, the two Adelaidean sections with obvious mixed siliciclastic prelude to cap carbonate deposition seem to permit that possibility.

Alternatively, postglacial, craton-derived sedimentation might precede the first appearance of cap carbonate if the time interval spanning basal Nuccaleena Formation siliciclastics represents the timescale of ocean buffering prior to build up of excess alkalinity (Hoffman *et al.* 1998; Higgins & Schrag 2003). Basal Nuccaleena Formation siliciclastic input might reflect local (tropical) deglaciation, as envisioned by Halverson *et al.* (2004)

while Nuccaleena Formation cap dolostone is synchronous with rapid global deglaciation.

Further elaboration of, and discrimination between, these hypotheses ought to be testable if basin-wide application of magnetic stratigraphy (or of any independent chronometer) seems robust—a scenario for which we lay a foundation in the remaining sections.

Rock magnetism

Cap carbonate coloration has largely driven regional, continental, and global correlation of associated Neoproterozoic ice ages; yet the origin of the (frequent, though not ubiquitous) 'pinkness' in cap units such as Nuccaleena Formation cap dolostone is not understood. Four scenarios are possible: (1) cap pinkness results from detrital iron oxides of sundry origin (eroded igneous, metamorphic, or second-cycle sedimentary, or biogenic/bioinduced in the aftermath of glaciation); (2) cap pinkness results from secondary iron oxide pigmentation—accompanying oxidation of organic matter originally present in caps but remineralized in the earliest diagenetic window, or accompanying chemical oceanographic changes during late diagenesis, post-lithification; (3) cap pinkness is a consequence of unique carbonate composition (e.g. Mn-rich dolomite) and is unrelated to iron-cycling; and (4) cap pinkness is a recent feature essentially induced by arid surficial weathering. This study favours a combination of the first and second hypotheses at the expense of the third, because terrigenous debris is ubiquitous in Nuccaleena Formation cap carbonate by direct observation and by rock-magnetic inference. The fourth is suggestively discounted, because recently pink cap dolostones have been described in quarry outcrop of a humid climate (Nogueira *et al.* 2003) and in Cenozoic mountaintop outcrop of a subalpine, temperate climate (Lorentz *et al.* 2004).

Environmental scanning electron microscopy and electron diffraction spectroscopy

Analyses of Nuccaleena Formation cap dolostone samples from the Elatina Creek and Trezona Bore sections reveal multiple non-carbonate phases, by rough order of abundance:

(1) equant iron oxide grains *c.* 0.1–100 microns in diameter, mode (O)10 microns;
(2) equant, low-Ti iron oxide grains *c.* 0.1–100 microns in diameter, mode (O)10 microns;
(3) nearly stoichiometric iron oxide grains $\ll$0.1 microns in diameter;
(4) Mg-clay;
(5) euhedral to subhedral rutile;
(6) well-rounded quartz;
(7) K-clay;
(8) subhedral to rounded apatite;
(9) relatively rare assemblages (REE-phosphate; botryoidal iron oxide or carbonate; zircon).

In Nuccaleena Formation cap dolostone, component-1 and -2 iron oxides, component-5 rutile, and component-6 quartz are ubiquitously rimmed by or adjacent to clays (Fig. 6b–h). Component-1 iron oxides are commonly concentrated in slightly undulose, bedding-parallel zones, without obvious grading (Fig. 6a). These zones are slightly undulose even when clearly not associated with stylolites. Supra-stylolite gangue might thicken in troughs and thin toward crests; but we have studied too few examples to generalize confidently. Nonetheless, Nuccaleena Formation cap dolostone clearly contains bedded iron oxides associated with other terrigenous mineral grains. If hematite or maghemite, these grains are expected to be of mostly single-domain size and therefore capable of recording a stable magnetization on geological timescales.

The smallest of the iron oxide size fraction observed (component-3) would also verge into the pseudo-single domain and single domain fields of magnetite. This crystal population is relatively scarce, though potential detection-limit imaging bias exists given the greater size and hence dominant conductivity/contrast of component-1 and -2 grains.

Component-3 iron oxide sometimes appears as 'salted, cloudy' sectors of clay platelets (Fig. 6e, h) and rarely, non-clay carbonate matrix (Fig. 6i).

Matrix carbonate textures are post-depositionally recrystallized; peloid margins, where visible in thick-section, are invisible under the eSEM. Small (mode *c.* 200 microns) dolomite rhombs dominate Nuccaleena Formation cap dolostone but vary size over of an order of magnitude. Low-Mn dolomite crystals are a minor component, and basal Trezona Bore carbonate (not figured) is more frequently zoned (calcite rims) than mid-Elatina Creek cap carbonate (rare, slightly zoned sector in Fig. 6i).

All Nuccaleena dolostone samples preserve occasional calcite rhombs mixed among dolomite rhombs, and also localize calcite to post-depositional textures, including subvertical, mildly tortuous zones. These calcite 'pipes' frequently crosscut macroscopic peloid lamination, and they sometimes feed, and are also often sourced by, calcite spar-filled sheet cracks. Rarely, a calcite pipe is upward-truncated by depositional peloid laminae. These pipes are interpreted as fluid escape structures active syn-depositionally and related to sheet crack growth and fill. Although recrystallization into pervasive rhomb fabric and calcification of some

rhomb rims certainly may have occurred long after Nuccaleena Formation cap dolostone was deposited, as calcite also appears to track these depositional sheet crack and pipe features, an early diagenetic origin can not be discounted.

Temperature dependence of magnetic susceptibility

Temperature dependences of low-field magnetic susceptibility, k(T), were measured on two Nuccaleena samples (macroscopically non-silty dolostone *c.* 2.5 m into solid cap carbonate at Enorama Creek GSSP; and spackly-weathering micrite, Brachina Formation interbed above solid dolostone at our Trezona Bore section; Table 1).

Changes in k(T) during warming from −192°C to room temperature in ambient atmosphere and cycling between room temperature and peak temperatures up to *c.* 720°C in flowing argon were measured using an AGICO KLY 4S magnetic susceptibility meter equipped with a high-temperature furnace and a cryostat. Repeated low-temperature warming runs, and successive heating-and-cooling runs to progressively higher peak temperatures were employed to document the temperature range and product character of the irreversible chemical reaction within cap dolostone more precisely, beginning between *c.* 330°C and 440°C (Fig. 7a, b, c).

For both samples, an inverse logarithmic decay of susceptibility, with a steep lowest-temperature tail, is observed during the initial warming-from-low-temperature run. Such behaviour suggests that magnetism of fresh Nuccaleena Formation cap dolostone is dominated by paramagnetic minerals (e.g. clays). A broad peak at *c.* −153°C on these low-temperature k(T) curves, associated with the Verwey transition (Verwey 1939) is hinted at by the initial Trezona Bore run, but not by the fresh Enorama Creek sample. Both samples, once thermally-altered by heating them to various temperatures, show Verwey transitions of varying definition, indicating the creation of near-stoichiometric magnetite.

No other magnetic transitions (such as hematite's Morin transition at *c.* −15°C [Morin 1950]) are observed. If hematite is present in either sample, it is also nonstoichiometric, or else smaller than *c.* 0.1 micron (Bando *et al.* 1965). eSEM analysis rules out the latter option.

When heated in argon, both samples show essentially reversible susceptibility at a *c.* 320°C peak temperature step. Elevated return susceptibility from *c.* 440°C and new presence of a broadened Verwey transition in the ensuing low-temperature warming run of Trezona Bore Nuccaleena document the onset of chemical reaction in that temperature interval. Steep susceptibility decrease in the *c.* 560°C–590°C range indicates presence of substantial magnetite by that point of the experiment, but absence of a well-expressed Hopkinson peak suggests that the magnetite is not single-domain (e.g. Dunlop 1974).

Further heating does not show a hematite signal (Néel temperature at *c.* 690°C), though cooling from peak temperatures above *c.* 580°C accentuates the near-stoichiometric magnetite signal (unblocking temperatures) and also creates at least one other phase, which ultimately stabilizes with distributed unblocking temperatures *c.* 250°C–400°C. We suspect this last phase is a manganese ferrite, which manifests similar behaviour during thermomagnetic analyses of synthetic and natural siderites (Isambert *et al.* 2003). The third local susceptibility maxima present on some runs, with peak susceptibility in the low 500°Cs, may be a metastable phase involved with the creation of the low-temperature ferrite.

Altogether, these changes suggest thermal lability of carbonate, including Mn-dolomite, in Nuccaleena Formation cap dolostone, with respect to an iron-bearing phase that is also initially present and labile. Magnetite may be created *de novo* from trace Fe-bearing carbonate (thus far unidentified by eSEM/EDS, although see unusual, interpreted microbialite phase, Fig. 7i, j) or from minor clay fractions in bulk Nuccaleena Formation cap dolostone, but almost surely, hematite and/or maghemite, if originally present in the rock, partly or wholly convert to magnetite beginning at *c.* 350°C. Carbon dioxide evolved from Nuccaleena Formation cap carbonate itself is likely the other major reactant, as carbonates undergo decarbonation reactions ('calcination' in the metallurgical literature, regardless of carbonate composition) between room temperature and *c.* 450°C, with reaction rates fixed by strong grain-size and weaker oxygen fugacity dependences (e.g. French & Rosenberg 1965).

As results of these experiments, we infer that magnetite, present in trace quantities of some pristine Nuccaleena Formation cap dolostone, should not contribute significantly to natural remanent magnetization; and is of generally <500 nm grain size (below the threshold of eSEM resolution). As eSEM imaging documents a significant clay component, yet ferromagnetic susceptibility does not show significant change across magnetite-evolving clay reaction temperatures (*c.* 120°C–170°C), it is likely that Nuccaleena Formation cap dolostone has been heated, *in situ*, to peak temperatures in or exceeding that range during its geological history. Any iron-bearing clay originally present has probably inverted, producing magnetite of ancient but secondary age (possibly evident in Fig. 7h, i). Such a thermal effect is plausible since

Fig. 8. Palaeomagic at the Ediacaran GSSP. Rock magnetic experiments described here seem to assure a detrital palaeomagnetic signal in Nuccaleena Formation cap dolostone, with or without overprinting by Ediacaran early diagenesis. Other studies document one, four, and one magnetic reversal during deposition of Walsh, Mirassol d'Oeste, and Hadash cap carbonates, potential 'Marinoan' correlative units to Nuccaleena Formation cap dolostone. If you were to wear 'magnetic goggles', the GSSP magnetic fingerprint might look something like this. White indicates 'reversed' polarity, directed SW and shallow upward, black indicates 'normal' polarity, directed NE and shallow downward, following polarity character and assignment of Sohl *et al.* (1999) for underlying Elatina Formation. Higher resolution sampling and pursuit of direct field tests of magnetization should better constrain the fidelity and interpretation of this signal.

the Ediacaran–Cambrian section above Nuccaleena Formation cap dolostone spans *c.* 3.5 km, of likely high geothermal gradient during Delamerian orogenesis.

Similarly, however, the change from reversible to irreversible susceptibility tracks between heating-to and cooling-from peak temperature runs beginning at *c.* 350°C establishes that as a maximum palaeothermometer constraint, if the phase reacting above 350°C is itself a primary component (Hrouda *et al.* 2003). Since the initial low-temperature experiments show only minor stoichiometric magnetite, and since the bulk susceptibility of unheated sample is low, hematite and/or maghemite are likely reactants during carbon dioxide volatilization. Continued production of magnetite from hematite and/or maghemite above 350°C possibly reflects kinetic limitation by the hematite and/or maghemite phase.

Magnetic hysteresis properties

Room-temperature hysteresis loops were collected using a Princeton Measurement vibrating sample magnetometer at the Institute of Rock magnetism (University of Minnesota) and a Princeton Measurement alternating gradient force magnetometer at the University of Rochester. Isothermal remanent magnetization (IRM) acquisition was performed on a 2G Enterprises™ DC-SQuID magnetometer in line with horizontal and vertical solenoids custom-built at California Institute of Technology, charged by a 2G capacitor relay box and modulated by custom-built transformer boxes.

Hysteresis loops on Nuccaleena Formation cap dolostone from *c.* 40 cm into the cap section at Elatina Creek, at a level where silt is still episodically visible to the naked eye, and from *c.* 2.1 m into the cap at Enorama Creek GSSP, where silt has mostly disappeared, are unsaturated at peak fields of *c.* 1.5 T (Fig. 7e, f). Consistent with initial low-temperature susceptibility experiments, both loops require significant paramagnetic corrections, indicating appreciable clay content. Upon correction, both samples exhibit wasp-waisted hysteresis (Fig. 7e, f), documenting presence of both a low-coercivity phase (like magnetite or maghemite) and a high-coercivity phase (goethite or hematite) in a ratio of at most 1:100 by saturation magnetization-corrected volume, respectively (Roberts *et al.* 1995; Tauxe *et al.* 1996).

IRM acquisition curves were measured for five Nuccaleena samples from various stratigraphic levels (Table 1) and for one upper Elatina, red sheet sandstone sample (collected from a section not otherwise described in this report—Bunyeroo Creek, at the southern margin of the continuous outcrop belt which includes Elatina Creek, Enorama Creek, and Trezona Bore).

All five cap carbonate curves cluster tightly and are dominated by a high-coercivity phase that is far from saturated at 370 mT (Fig. 7 g), the maximum field available using our equipment. The high-field slopes of remanence acquisition are higher than expected for goethite, marking hematite as the dominant high-coercivity phase (France & Oldfield 2000). The red sheet sandstone also yields a magnetically hard IRM acquisition spectrum, but one clearly mixed with a broad fraction of low-coercivity grains, probably clay-associated magnetite. Interestingly, the magnetically softest of the tightly clustered cap carbonate group is the single cap carbonate sample that also comes from Bunyeroo Creek, a section which is strongly tectonized and somewhat weathered with respect to the others. Of all Nuccaleena sections reported here, our secondary magnetite hypothesis described above would predict most secondary magnetite at Bunyeroo Creek.

Since eSEM imaging documents bedding-parallel layers of abundant iron oxide grains larger than the single-domain stability field of magnetite, all rock magnetic experiments described herein point to hematite as the dominant ancient carrier of detrital magnetization. Since hematite is documented as a detrital component carrying primary magnetization in underlying Elatina Formation and overlying Brachina siltstone, and since abundant hematite may be sourced from Palaeoproterozoic banded iron formations or Mesoproterozoic hydrothermal breccia deposits exposed on Gawler craton, we interpret detrital hematite to dominate Nuccaleena natural remanence and plausibly preserve primary magnetization.

Since thermomagnetic evolution experiments establish *c.* 330°C as a maximum estimate for peak palaeotemperature, any Ediacaran hematite magnetization will be preserved to the present unless chemically altered. At present, we cannot distinguish hematite pigments, possibly formed on the surface of detrital hematite grains while Nuccaleena Formation cap dolostone was still in the diagenetic window, from exclusively detrital hematite. Delamerian and younger pigments are largely ruled out, as they would coat quartz and carbonate grains as well as opaque crystals. Therefore magnetite remanence, if extractable during demagnetization, should be largely secondary, and higher unblocking-temperature phases should be purely detrital or a mixture of detrital and early diagenetic magnetization.

Discussion

For any rock of this assemblage, laboratory characterization of that compound remanence can be challenging. Alternating field demagnetization cannot

isolate characteristic magnetization alone, since goethite and hematite both will be unaffected. As documented in the thermosusceptibility section above, however, wholly thermal demagnetization is likely to destroy the very particles carrying primary remanence, and create new ferromagnetic grains locking in laboratory remanences with blocking temperatures appropriate to the oxygen fugacity of the demagnetizing furnace. It might be difficult to distinguish this laboratory magnetite remanence from that carried by geologic, secondary magnetite in a cap carbonate.

Context

Some of these concerns are voiced by Font *et al.* (2005), who undertake a similar SEM–rock magnetics study on Mirassol d'Oeste cap dolostone in Brazil. We confirm their findings: that pink cap dolostones contain micron-diameter iron oxide grains with bedded texture, most likely hematite because of high coercivity; that irreversible chemical reactions occur upon heating; and that clay is closely associated with iron-bearing phases, on the scale of an EDS analysis (see their fig. 9).

The conclusion applied to the Mirassol d'Oeste cap (that magnetite is a likely detrital magnetization carrier) is not shared. It seems difficult to rule out secondary origin of magnetite without independent palaeothermometry. With this minor exception, we replicate the findings of Font *et al.* (2005) and augment them by applying thermal-dependence of susceptibility reversibility as a palaeothermometer for low-grade burial metamorphism of Nuccaleena Formation cap carbonate; by documenting at least two distinct thermal reaction products in flowing argon atmosphere; and by determining the temperature ranges of those reactions.

Li (2000) presaged both petrophysical studies by noting thin, red silt stringers common in Walsh cap carbonate samples from Western Australia's Kimberley region and suggesting that detrital hematite accounts for Marinoan cap 'pinkness.' His findings are supported by the documenting here of detrital hematite grains in unerring association with clay flocs as well as commonly with detrital quartz and rutile, in cap carbonate facies where no red silt is apparent to the naked eye. It is suggested that the *c.* 300°C instability (sample explosions in the furnace; acquisition of anomalous magnetizations) Li (2000) noted in *c.* 50% of samples, and the similar instability previously reported to account for unsuccessful palaeomagnetic investigation of Nuccaleena Formation (Sohl *et al.* 1999, supplementary data) are due to ferric reduction (and possibly re-oxidation) accompanying carbon dioxide devolatilization of carbonate samples in that temperature range.

Kilner *et al.* (2005) figure orthogonal demagnetization vector diagrams that unblock by *c.* 600°C or by *c.* 690°C. Without knowing the lithologic identity of those specimens, and in the absence of other petrographic or rock-magnetic data published to-date from Oman's Hadash cap, it is difficult to assess the extent to which these interpretations apply to that study.

Several hybrid demagnetization strategies have been attempted here, designed to isolate carriers of each natural- or laboratory-induced remanence, on Nuccaleena Formation cap dolostone, with varying success (Fig. 8). If direct field tests of Nuccaleena magnetization were to demonstrate ancient origin of a particular component, considerable light would be shed on the robustness of that and other palaeomagnetic results from cap carbonates worldwide.

Conclusions

Nuccaleena Formation cap dolostone was deposited in varying thickness along strike of a single outcrop belt during the terminal phase of Elatina–Nuccaleena deglaciation. This terminal deglaciation began amid widespread erosion, and accommodation space preserved on the flank of a salt diapir or in deep-water settings recorded siliciclastic input of pulsed or prolonged character, with accompanying or episodic episodes of renewed erosion during deposition of 'red sheet sandstone'. These erosive episodes might have occupied intervals when ongoing isostatic rebound temporarily outpaced eustatic transgression. Later influx of alkalinity is separable from physical onset of ultimate deglaciation, and it may have been sourced by deep water upwelling, in the simplest lithostratigraphic correlation scheme presented here.

The Ediacaran GSSP is not marked at the basal Wilpena Group unconformity, as intended, but fully *c.* $\frac{1}{3}$ of the way through the terminal deglacial sequence at the very sections in Flinders Ranges showing clearest evidence for low-palaeolatitude Elatina glaciation.

Terrigenous input continued to those sections during deposition of Nuccaleena Formation cap carbonate, possibly decoupled from shale input. Detrital hematite is expected to record a faithful, stable magnetization in Nuccaleena Formation cap dolostone and other 'pink' cap carbonates, but elucidation of detrital versus early diagenetic magnetizations will be challenging for conventional palaeomagnetic laboratory techniques.

The authors acknowledge support from the Australian Research Council through its Research Centres Program, the David and Lucile Packard Foundation, and the National Science Foundation Graduate Research Fellowship Program. Critical reviews by W. Preiss and P. Betts

and informal reviews by A. Maloof, B. Kopp, and E. Sperling greatly improved the manuscript. Discussions in the field with T. Prave, N. Christie-Blick, J. Gehling, R. Petterson, and B. Wernicke; and out of it with D. Kent, R. Trindade, P. Hoffman, A. Kosterov, and M. Kennedy improved the authors' understanding of complications and caveats. Field work in Flinders Ranges National Park was particularly facilitated by K. Anderson, N. di Preu, and P. Canty of Parks and Wildlife South Australia, by R. Coulthard and P. Coulthard of the Flinders Ranges Aboriginal Heritage Consultative Committee Inc; and by able field assistantship from C. Izard and I. Howley. This paper is publication #390 of the Tectonics Special Research Centre and a contribution to International Geological Correlation Program (IGCP) 493 and 512.

References

ALLEN, P. A. & HOFFMAN, P. F. 2005. Extreme winds and waves in the aftermath of a Neoproterozoic glaciation. *Nature*, **433**, 123–127.

BANDO, Y., KIYAMA, M., YAMAMOTO, N., TAKADA, T., SHINJO, T. & TAKAKI, H. 1965. Magnetic properties of alpha-Fe_2O_3 fine particles. *Journal of the Physical Society of Japan*, **20**, 2086.

BODISELITSCH, B., KOEBERL, C., MASTER, S. & REIMOLD, W. U. 2005. Estimating intensity and duration of Neoproterozoic snowball glaciations from Ir anomalies. *Science*, **308**, 239–242.

CALLEN, R. A. & REID, P. W. 1994. Geology of the Flinders Ranges National Park. *South Australia Geological Survey. Special Map*, 1:75 000.

CELERIER, J., SANDIFORD, M., HANSEN, D. L. & QUIGLEY, M. 2005. Modes of active intraplate deformation, Flinders Ranges, Australia. *Tectonics*, **24**, Art. No. TC6006. DOI: 10.1029/2004TC001679, 2005.

CHETEL, L. M., SIMO, J. A. & SINGER, B. S. 2005. 40-Ar/39-Ar geochronology and provenance of detrital K-feldspars, Ordovician, Upper Mississippi Valley. *Sedimentary Geology*, **182**, 163–181.

CHRISTIE-BLICK, N., DYSON, I. A. & VON DER BORCH, C. C. 1995. Sequence stratigraphy and the interpretation of Neoproterozoic Earth history. *Precambrian Research*, **73**, 3–26.

DUNLOP, D. J. 1974. Thermal enhancement of magnetic susceptibility. *Journal of Geophysics*, **40**, 439–451.

DYSON, I. A. 1992. Stratigraphic nomenclature and sequence stratigraphy of the lower Wilpena Group, Adelaide Geosyncline; the Sandison Subgroup. *Quarterly Geological Notes of the Geological Survey of South Australia*, **122**, 2–13.

EMBLETON, B. J. J. & WILLIAMS, G. E. 1986, Low paleolatitude of deposition for Late Precambrian periglacial varvites in South Australia—Implications for paleoclimatology. *Earth and Planetary Science Letters*, **79**, 419–430.

EVANS, D. A. D. 2000. Stratigraphic, geochronological, and paleomagnetic constraints upon the Neoproterozoic climatic paradox. *American Journal of Science*, **300**, 347–433.

FONT, E., TRINDADE, R. I. F. & NÉDÉLEC, A. 2005. Detrital remanent magnetization in haematite-bearing Neoproterozoic Puga cap dolostone, Amazon craton: a rock magnetic and SEM study. *Geophysical Journal International*, **163**, 491–500.

FRANCE, D. E. & OLDFIELD, F. 2000. Identifying goethite and hematite from rock magnetic measurements of soils and sediments. *Journal of Geophysical Research*, **105**, 2781–2795.

FRENCH, B. M. & ROSENBERG, P. E. 1965. Siderite ($FeCO_3$)—thermal decomposition in equilibrium with graphite. *Science*, **147**, 1283.

GEHRELS, G. E., BUTLER, R. F. & BAZARD, D. R. 1996. Detrital zircon geochronology of the Alexander terrane, southeastern Alaska. *Geological Society of America Bulletin*, **108**, 722–734.

GOODMAN, J. C. & PIERREHUMBERT, R. T. 2003. Glacial flow of floating marine ice in 'Snowball Earth.' *Journal of Geophysical Research*, **108**, Art. No. 3308. DOI: 10.1029/2002JC001471, 2003.

GROTZINGER, J. P. & KNOLL, A. H. 1995. Anomalous carbonate precipitates: Is the Precambrian the key to the Permian? *Palaios*, **10**, 578–596.

HALVERSON, G. P., MALOOF, A. C. & HOFFMAN, P. F. 2004. The Marinoan glaciation (Neoproterozoic) in northeast Svalbard. *Basin Research*, **16**, 297–324.

HIGGINS, J. A. & SCHRAG, D. P. 2003. Aftermath of a snowball Earth. *Geochemistry, Geophysics, Geosystems*, **4**, Art. No. 1028. DOI: 10.1029/2002GC000403.

HOFFMAN, P. F. 2005. 28th DeBeers Alex Du Toit Memorial Lecture: On Cryogenian (Neoproterozoic) ice-sheet dynamics and the limitations of the glacial sedimentary record. *South African Journal of Geology*, **108**, 557–577.

HOFFMAN, P. F. & SCHRAG, D. P. 2002. The snowball Earth hypothesis: testing the limits of global change. *Terra Nova*, **14**, 129–155.

HOFFMAN, P. F., KAUFMAN, A. J., HALVERSON, G. P. & SCHRAG, D. P. 1998. A Neoproterozoic snowball Earth. *Science*, **281**, 1342–1346.

HROUDA, F., MÜLLER, P. & HANÁK, J. 2003. Repeated progressive heating in susceptibility vs. temperature investigation: a new palaeotemperature indicator? *Physics and Chemistry of the Earth*, **28**, 653–657.

HYDE, W. T., CROWLEY, T. J., BAUM, S. K. & PELTIER, W. R. 2000. Neoproterozoic 'Snowball Earth' simulations with a coupled climate/ice-sheet model. *Nature*, **405**, 425–429.

ISAMBERT, A., VALET, J. P., GLOTER, A. & GUYOT, F. 2003. Stable Mn-magnetite derived from Mn-siderite by heating in air. *Journal of Geophysical Research*, **108**, Art. No. 2283. DOI: 10.1029/2002JB002099, 2003.

JAMES, N. P., NARBONNE, G. M. & KYSER, T. K. 2001. Late Neoproterozoic cap carbonates: Mackenzie Mountains, northwestern Canada: precipitation and global glacial meltdown. *Canadian Journal of Earth Sciences*, **38**, 1229–1262.

KASEMANN, S. A., HAWKESWORTH, C. J., PRAVE, A. R., FALLICK, A. E. & PEARSON, P. N. 2005. Boron and calcium isotope composition in Neoproterozoic carbonate rocks from Namibia: evidence for extreme environmental change. *Earth and Planetary Science Letters*, **231**, 73–86.

KENNEDY, M. J. 1996. Stratigraphy, sedimentology, and isotopic geochemistry of Australian Neoproterozoic

postglacial cap dolostones: Deglaciation, δC-13 excursions, and carbonate precipitation. *Journal of Sedimentary Research*, **66**, 1050–1064.

KENNEDY, M. J., RUNNEGAR, B., PRAVE, A. R., HOFFMANN, K. H. & ARTHUR, M. A. 1998. Two or four Neoproterozoic glaciations? *Geology*, **26**, 1059–1063.

KENNEDY, M. J., CHRISTIE-BLICK, N. & PRAVE, A. R. 2001. Carbon isotopic composition of Neoproterozoic glacial carbonates as a test of paleooceanographic models for snowball Earth phenomena. *Geology*, **29**, 1135–1138.

KILNER, B., MAC NIOCAILL, C. & BRASIER, M. 2005. Low-latitude glaciation in the Neoproterozoic of Oman. *Geology*, **33**, 413–416.

KIRSCHVINK, J. L. 1992. Late Proterozoic Low-Latitude Global Glaciation: The Snowball Earth. *In*: SCHOPF, J. W., KLEIN, C. & DES MARAIS, D. (eds) *The Proterozoic Biosphere: A Multidisciplinary Study*. Cambridge University Press, 51–52.

KNOLL, A. H., WALTER, M. R., NARBONNE, G. M. & CHRISTIE-BLICK, N. 2004. A new period for the geologic time scale. *Science*, **305**, 621–622.

KNOLL, A. H., WALTER, M. R., NARBONNE, G. M. & CHRISTIE-BLICK, N. 2006. The Ediacaran Period: a new addition to the geologic time scale. *Lethaia*, **39**, 13–30.

LEMON, N. M. 2000. A Precambrian fringing stromatolite reef complex, Flinders Ranges, South Australia. *Precambrian Research*, **100**, 109–120.

LEMON, N. M. & GOSTIN, V. A. 1990. Glacigenic sediments of the late Proterozoic Elatina Formation and equivalents, Adelaide Geosyncline, South Australia. *In*: JAGO, J. B. & MOORE, P. S. (eds) *The Evolution of a Late Precambrian–Early Palaeozoic Rift Complex: The Adelaide Geosyncline*. Geological Society of Australia Special Publication, **16**, 149–163.

LI, Z. X. 2000. New palaeomagnetic results from the 'cap dolomite' of the Neoproterozoic Walsh Tillite, northwestern Australia. *Precambrian Research*, **100**, 359–370.

LORENTZ, N. J., CORSETTI, F. A. & LINK, P. K. 2004. Seafloor precipitates and C-isotope stratigraphy from the Neoproterozoic Scout Mountain Member of the Pocatello Formation, southeast Idaho: implications for Neoproterozoic earth system behavior. *Precambrian Research*, **130**, 57–70.

MARSHAK, S. & FLOTTMANN, T. 1987. Structure and origin of the Fleurieu and Nackara arcs in the Flinders fold-thrust belt, south Australia: Salient and recess development in the Delamerian Orogen. *Journal of Structural Geology*, **18**, 891–908.

MORIN, F. J. 1950. Magnetic susceptibility of αFe_2O_3 and αFe_2O_3 with added titanium. *Physical Reviews*, **78**, 819–820.

NOGUEIRA, A. C. R., RICCOMINI, C., SIAL, A. N., MOURA, C. A. V. & FAIRCHILD, T. R. 2003. Soft-sediment deformation at the base of the Neoproterozoic Puga cap carbonate (southwestern Amazon Craton, Brazil): confirmation of rapid icehouse-greenhouse transition in snowball earth. *Geology*, **31**, 613–616.

PIERREHUMBERT, R. T. 2005. Climate dynamics of a 'hard' snowball Earth. *Journal of Geophysical Research*, **110**, Art. No. D01111. DOI: 10.1029/2004JD005162.

PLUMMER, P. S. 1979. Note on the palaeoenvironmental significance of the Nuccaleena Formation (upper Precambrian), central Flinders Ranges, South Australia. *Journal of the Geological Society of Australia*, **25**, 395–402.

POLLARD, D. & KASTING, J. F. 2005. Snowball Earth: a thin-ice solution with flowing sea glaciers. *Journal of Geophysical Research*, **110**, Art. No. C07010. DOI: 10.1029/2004JC002525.

PREISS, W. V. 1987. The Adelaide Geosyncline—late Proterozoic stratigraphy, sedimentation, palaeontology and tectonics. *Geological Survey of South Australia, Bulletin*, **53**.

PREISS, W. V. 1990. A stratigraphic and tectonic overview of the Adelaide Geosyncline, South Australia. *In*: JAGO, J. B. & MOORE, P. S. (eds) *The Evolution of a Late Precambrian-Early Palaeozoic Rift Complex: The Adelaide Geosyncline*. Geological Society of Australia Special Publication, **16**, 1–33.

PREISS, W. V. 1992. The Ketchowla Siltstone and Stratigraphy of the Marinoan Glacial Yerelina Subgroup. *Quarterly Geological Notes of the Geological Survey of South Australia*, **121**, 7–15.

PREISS, W. V. 1993. Neoproterozoic. *In*: DREXEL, J. F., PREISS, W. V. & PARKER, A. J. (eds) *The Geology of South Australia. Vol. 1, The Precambrian*. Geological Survey of South Australia, Bulletin, **54**, 171–202.

PREISS, W. V. 2000. The Adelaide Geosyncline of South Australia and its significance in Neoproterozoic continental reconstruction. *Precambrian Research*, **100**, 21–63.

PREISS, W. V. 2005. Global stratotype for the Ediacaran System and Period—the golden spike has been placed in South Australia. *MESA Journal*, **37**, 20–25.

PREISS, W. V., DYSON, I. A., REID, P. W. & COWLEY, W. M. 1998. Revision of lithostratigraphic classification of the Umberatana Group. *MESA Journal*, **9**, 36–42.

REMANE, J. & ADATTE, T. 2002. Foreword. *Palaeogeography, Palaeoclimatology, Palaeoecology*, **178**, 137.

ROBERTS, A. P., CUI, Y. L. & VEROSUB, K. L. 1995. Wasp-waisted hysteresis loops—mineral magnetic characteristics and discrimination of components in mixed magnetic systems. *Journal of Geophysical Research*, **100**, 17909–17924.

SCHMIDT, P. W. & WILLIAMS, G. E. 1995. The Neoproterozoic climatic paradox; equatorial palaeolatitude for Marinoan Glaciation near sea level in South Australia. *Earth and Planetary Science Letters*, **134**, 107–124.

SCHMIDT, P. W., WILLIAMS, G. E. & EMBLETON, B. J. J. 1991. Low palaeolatitude of late Proterozoic glaciation; early timing of remanence in haematite of the Elatina Formation, South Australia. *Earth and Planetary Science Letters*, **105**, 355–367.

SHIELDS, G. A. 2005. Neoproterozoic cap carbonates: a critical appraisal of existing models and the plume-world hypothesis. *Terra Nova*, **17**, 299–310.

SOHL, L. E., CHRISTIE-BLICK, N. & KENT, D. V. 1999. Paleomagnetic polarity reversals in Marinoan (ca. 600 Ma) glacial deposits of Australia; implications for the

duration of low-latitude glaciation in Neoproterozoic time, *Geological Society of America Bulletin*, **111**, 1120–1139.

SUMNER, D. Y., KIRSCHVINK, J. L. & RUNNEGAR, B. N. 1987. Soft-sediment paleomagnetic field tests of late Precambrian glaciogenic sediments. *EOS, Transactions of the American Geophysical Union*, **68**, 1251.

TAUXE, L., MULLENDER, T. A. T. & PICK, T. 1996. Potbellies, wasp-waists, and superparamagnetism in magnetic hysteresis. *Journal of Geophysical Research*, **101**, 571–583.

TRINDADE, R. I. F., FONT, E., D'AGRELLA-FILHO, M. S., NOGUEIRA, A. C. R. & RICCOMINI, C. 2003. Low-latitude and multiple geomagnetic reversals in the Neoproterozoic Puga cap carbonate, Amazon craton. *Terra Nova*, **15**, 441–446.

VERWEY, E. J. W. 1939. Electron conduction of magnetite (Fe_3O_4) and its transition point at low temperatures. *Nature*, **144**, 327–328.

WARREN, S. G., BRANDT, R. E., GRENFELL, T. C. & MCKAY, C. P. 2002. Snowball Earth: ice thickness on the tropical ocean. *Journal of Geophysical Research*, **108**, Art. No. 31. DOI: 10.1029/2001JC001123.

WILLIAMS, G. E. 1979. Sedimentology, stable-isotope geochemistry and palaeoenvironment of dolostones capping late Precambrian glacial sequences in Australia. *Journal of the Geological Society of Australia*, **26**, 377–386.

WILLIAMS, G. E. & TONKIN, D. G. 1985. Periglacial structures and palaeoclimatic significance of a late Precambrian block field in the Cattle Grid copper mine, Mount Gunson, South Australia. *Australian Journal of Earth Sciences*, **32**, 287–300.